# ELECTROPHYSIOLOGICAL COMPARISON OF $Na_V1.5$ EXPRESSED IN HEK293 CELLS TO NATIVE $Na_V$ CURRENTS IN CARDIAC MYOCYTES

by

William Corey Valinsky

A thesis submitted to the Physiology Graduate Program in the

Department of Biomedical and Molecular Sciences

in conformity with the requirements for

the degree of Master of Science

Queen's University

Kingston, Ontario, Canada

(August, 2011)

# Abstract

Contraction of cardiac muscle is a highly regulated event that relies on a delicate balance of ions entering and leaving the cell through ion channels. In particular, voltage gated sodium channels are responsible for the rapid depolarization that leads to a contraction. During an oxidative challenge, sodium channels rapidly activate, but do not fully turn off. This alters the rate of cardiac repolarization and can induce cardiac arrhythmias. It is currently unknown whether the most common sodium channel isoform found in the heart, $Na_V1.5$, generates this oxidant-induced persistent current or if other isoforms are responsible. Therefore, I sought to further explore the biophysical properties $Na_V1.5$, and determine if it can enter this persistent mode.

I tested the biophysical properties of native $I_{Na}$ in cardiac myocytes and in $Na_V1.5$ transfected HEK293 cells under macro cell-attached voltage-clamp. I used a sodium channel enhancer (*Anemonia sulcata* toxin II; 10 nM), a sodium channel blocker (tetrodotoxin; 10 nM) and a model of oxidative stress ($H_2O_2$; 100 μM, 200 μM, 1000 μM) to compare and contrast the cellular responses between both cell types. I observed that transfected HEK293 cells and cardiac myocytes were unaffected by $H_2O_2$ at various concentrations. Given the lack of other isoforms in transfected HEK293 cells, and the low abundance (<5%) of other isoforms in cardiac myocytes, I propose that $Na_V1.5$ function is unaffected by $H_2O_2$. Furthermore, ATX II prolonged the inactivation process in both HEK293 cells and cardiac myocytes in a voltage-dependent manner, indicating that $Na_V1.5$ can give rise to persistent sodium current. Finally, by comparing both cell types under control settings, I found that transfected HEK293 cells inactivated at a much slower rate and at more negative potentials compared to the current in cardiac myocytes. My results suggest that $Na_V1.5$ does not underlie oxidant-induced persistent current and that β subunits likely play a significant role in the inactivation process.

# Acknowledgements

First and foremost, I'd like to thank Dr. Christopher Ward for his teaching, guidance and assistance in my graduate program. I'd also like to thank the other members of the Ward lab for their help, patience and support over the last two years. To Sarah, thanks for taking the time to teach me how to operate a patch clamp rig, work the always-dysfunctional pipette puller while providing plenty laughs along the way. To Gina, thanks for helping me get a grip on HEK293 cell culture and being supportive during the rough days of contaminations and poor transfection rates. I'll also fondly remember our never-ending debate on the appropriate methods of fitness and training, even though one of us never convinced the other that we were right.

I'd also like to thank Shetuan Zhang and his entire lab for countless resources and time spent assisting me over the last two years. Specifically, Jun Guo, for providing me with plenty of assistance with bacterial transformations, maxi-prep isolations and HEK293 cell transfections. Without your help, there is no way this project would've ever taken off.

Finally, I'd like to thank family and friends for their continued support over the years. To my parents, thanks for helping to ensure that my rent cheques didn't bounce and always showing an interest in my work, even though I never successfully explained to you what I did.

# Table of Contents

# List of Figures

# List of Tables

# Abbreviations

| | |
|---|---|
| °C | Degrees Celsius |
| % | Percent |
| α | Alpha |
| β | Beta |
| μ | Micro |
| Ω | Ohm |
| A | Alanine |
| ATX II | *Anemonia sulcata* Toxin II |
| $Ba^{2+}$ | Barium |
| C | Cysteine |
| $Ca^{2+}$ | Calcium |
| CNS | Central Nervous System |
| D# | Domain number (1-4) of a VGSC |
| D | Aspartic Acid |
| $_{dd}H_2O$ | Double Distilled Water |
| DAD | Delayed afterdepolarization |
| E | Glutamic Acid |
| EAD | Early afterdepolarization |
| g | Gram |
| GFP | Green Fluorescent Protein |
| $H_2O_2$ | Hydrogen Peroxide |
| Hz | Hertz |
| IFM | Isoleucine, phenylalanine, methionine |
| $I_{Na}$ | Sodium Current |
| $I_{Na(T)}$ | Transient Sodium Current |
| $I_{Na(P)}$ | Persistent Sodium Current |
| IR | Ischemia-reperfusion |
| IV | Current-Voltage |
| $K^+$ | Potassium |
| K | Lysine |
| k | Kilo |
| KB | Kraft-Brühe |
| L | Litre |
| LQT3 | Long Q-T Syndrome Type 3 |
| m | Milli |
| MI | Myocardial Infarction |
| min | Minutes |
| mm | Millimeter |
| $Na^+$ | Sodium |
| $Na_V1.\#$ | VGSC Isoform number (1-9) |

| | |
|---|---|
| NCX | Sodium-Calcium Exchanger |
| pA | PicoAmpere |
| PKA | Protein Kinase A |
| PKC | Protein Kinase C |
| ROS | Reactive Oxygen Species |
| S# | Transmembrane domain number (1-6) of a VGSC |
| S.E.M | Standard Error of the Mean |
| s | Seconds |
| SA | Sinoatrial |
| STX | Saxitoxin |
| TTX | Tetrodotoxin |
| V | Volts |
| $V_{50}$ | Voltage of 50% Inactivation |
| $V_C$ | Command Potential |
| $V_H$ | Holding Potential |
| VGSC | Voltage Gated Sodium Channel |

# Chapter 1

# Introduction and Literature Review

## Voltage Gated Sodium Channels

Voltage gated sodium channels (VGSCs) are integral membrane proteins responsible for the influx of sodium ions into a cell (Yu & Catterall, 2003), and are critical in the initiation and propagation of action potentials in excitable cells (Hodgkin & Huxley, 1952), such as neurons and cardiac myocytes. Hodgkin and Huxley (1952) first identified that these channels open in response to membrane depolarization, inactivate shortly thereafter, and exhibit selective ion conductance. It is now known that VGSCs are large multimeric proteins consisting of a pore forming α subunit and multiple non-identical β subunits (Hartshorne *et al.*, 1982; Yu & Catterall, 2003; Figure 1).

Sodium ion conductance through VGSCs occurs entirely via the α subunit (Yu & Catterall, 2003). The α subunit is a 260 kDa complex composed of four homologous domains (D1-D4), each consisting of six transmembrane domains (S1-S6) (Hartshorne *et al.*, 1982). The four domains are believed to fold together and form a circular pore located between all S5 and S6 segments (Bezanilla, 2000). A re-entrant loop located in the transmembrane region of the channel (between S5-S6 in all domains) forms the ion-selectivity filter in the outer pore (Catterall, 2000). Two charged amino acids in analogous positions across all four domains are believed to form the inner and outer rings of the ion selectivity filter (Yu & Catterall, 2003). This was elegantly shown in a mutagenesis study where a calcium-selective VGSC was produced by mutating the inner ring residues aspartic acid (D) in D1, glutamic acid (E) in D2, lysine (K) in D3, and alanine (A) in D4

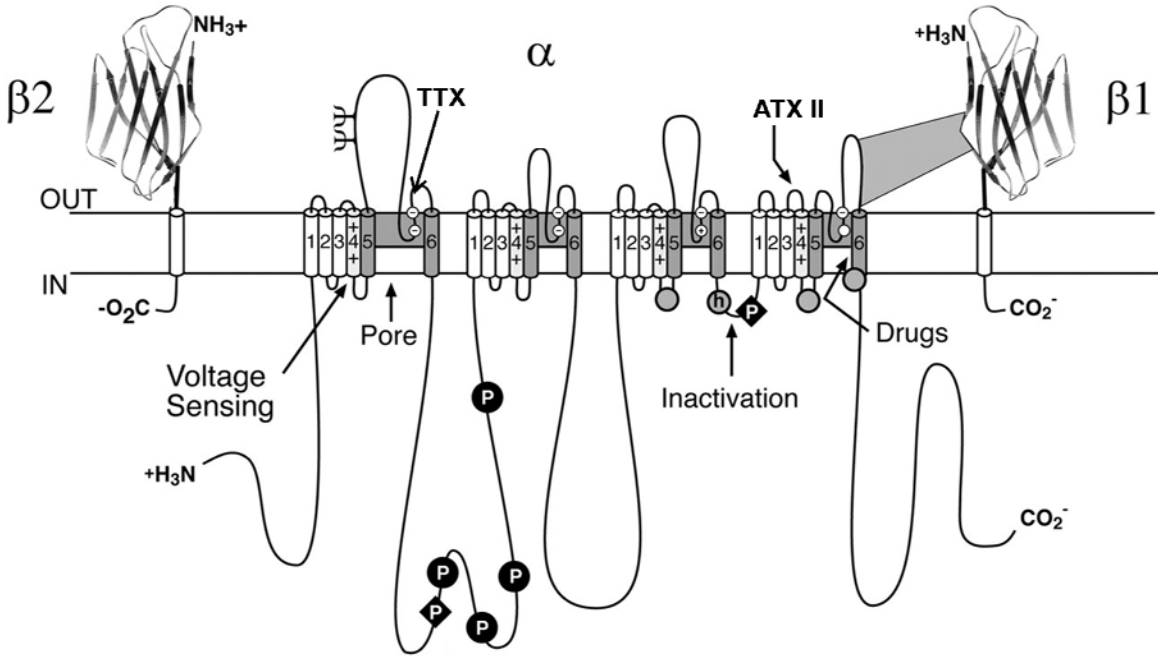


**Figure 1**: **Structure of Voltage Gated Sodium Channels.** The primary structures of the subunits of the voltage-gated sodium channel are illustrated as transmembrane folding diagrams. Cylinders represent probable α-helical segments. Bold lines represent the polypeptide chains of each subunit with length approximately proportional to the number of amino acid residues in the brain sodium channel subtypes. The extracellular domains of the β1 and β2 subunits are shown as immunoglobulin-like folds. ψ, sites of probable N-linked glycosylation; P in circles, sites of demonstrated protein phosphorylation by PKA (circles) and PKC (diamonds); Sites of binding of ATX II, TTX and a site of interaction between α and β1 subunits are also shown. (modified from Catterall, 2000).

to EEEE (Heinemann *et al.*, 1992b). The respective residues located in the outer ring are EEDD (Docherty & Farmer, 2009).

There are currently nine VGSC α subunits that have been identified and functionally expressed ($Na_v1.1$, $Na_v1.2$, $Na_v1.3$, $Na_v1.4$, $Na_v1.5$, $Na_v1.6$, $Na_v1.7$, $Na_v1.8$, $Na_v1.9$; Catterall *et al.*, 2005). Each channel is named after the gene that encodes its α subunit (Catterall *et al.*, 2005), which are SCN1A-SCN5A and SCN8A-SCN11A (Goldin, 1999). These nine channels have been shown to have greater than 50% amino acid homology (Catterall *et al.*, 2005).

Voltage-dependent activation of VGSCs derives from the outward movement of charged residues as a result of an altered electrical field across the membrane (Hodgkin & Huxley, 1952). Initial tests into voltage-dependent activation pointed to the S4 voltage sensor being critical for the process; whereby neutralization of the positively charged residues in the S4 segment caused a marked reduction of voltage-dependent activation (Stuhmer *et al.*, 1989). Specifically, each S4 segment consists of one positively charged amino acid, followed by two hydrophobic amino acids, possibly forming an α-helix motif (Bezanilla, 2000). These positively charged amino acids are believed to cause the S4 segment to rotate outwards during a depolarization, which pulls the S5 segment and opens a space between S5 and S6 for sodium ions to pass through (Catterall, 2000).

Inactivation of VGSCs usually occurs within milliseconds of opening. It is generally accepted that a highly conserved intracellular loop located between S6 of D3 and S1 of D4 physically blocks the intracellular pore (Catterall, 2000). This 'fast inactivation' is believed to be coupled to activation, whereby movement of the voltage sensor immediately engages the inactivation plug and, thus, ionic flow is ceased (Catterall, 2000). Mutagenesis studies have confirmed that three key hydrophobic amino acids are required for fast inactivation; isoleucine,

phenylalanine and methionine (IFM) (West *et al.*, 1992). Structural analysis of the inactivation gate has revealed that it is a rigid α-helix flanked on its N-terminal side by two turns, the second turn containing the IFM motif (Rohl *et al.*, 1999). A unique feature of this structure is that the phenylalanine residue of the IFM motif projects away from the helix (Catterall, 2000). Under most circumstances, hydrophobic amino acids, such as phenylalanine, are typically bundled in the center of the protein, far away from water. This strongly suggests that the phenylalanine residue of the IFM motif is responsible for blocking the intracellular pore during fast inactivation (Catterall, 2000). Sodium channels can also inactivate through slow inactivation and ultra slow inactivation (Goldin, 2003). These are believed to inactive the channel via rearrangement of the pore, however the exact mechanisms underlying these methods of inactivation are poorly understood (Goldin, 2003).

Early voltage clamp studies did not reveal any modulation of sodium channels via second messengers, however, biochemical studies have shown that VGSCs are readily phosphorylated by cAMP-dependent protein kinases, thereby reducing their ion conductance (Costa & Catterall, 1984a). Further biochemical analysis identified that sodium channels are phosphorylated at four sites on a large intracellular loop between S6 of D1 and S1 of D2 (Murphy *et al.*, 1993). Phosphorylation via protein kinase A (PKA; Rossie & Catterall, 1987) was shown to reduce peak inward current without substantially affecting activation or inactivation kinetics (Li *et al.*, 1992). On the contrary, phosphorylation via protein kinase C (PKC; Costa & Catterall, 1984b) was shown to not only reduce peak current, but also slow sodium channel inactivation (Numann *et al.*, 1991). PKC is able to modulate inactivation kinetics of the channel because it phosphorylates the protein at two sites: 1) at the inactivation gate and 2) on the intracellular loop between D1-D2

(West *et al.*, 1991). By having a direct influence on the inactivation gate of VGSCs, PKC is able to modulate the inactivation kinetics of VGSCs.

The β subunits of VGSCs are believed to be involved in modulating channel gating and cell-cell interactions (Catterall, 2000). Four β subunits have been identified to date, with β1 and β2 being expressed in the brain (Catterall *et al.*, 2005), while β1 is expressed in the atria/ventricles and β3 in the ventricles/Purkinje fibres (Fahmi *et al.*, 2001). Thus, ventricular myocytes coexpress β1 and β3 subunits. Currently, there are few experiments that directly test the effect of β subunits and their role in cell-cell communications. As stated earlier, the β subunits are capable of modulating channel gating. This was first observed in cells that were β subunit deprived; these cells inactivated at a much slower rate in comparison to cells containing β subunits (Schreibmayer *et al.*, 1994). It was determined through further analysis that the extracellular loop between S5-S6 of D1 and D4 interacts with the extracellular fold of the β1 subunit (Makita *et al.*, 1996) to modulate gating via an unknown mechanism.

## VGSC Blockers: Tetrodotoxin and Saxitoxin

Tetrodotoxin (TTX) and saxitoxin (STX) are marine toxins that selectively block VGSCs with high affinity (Fozzard & Lipkind, 2010). Both are potentially lethal toxins as they inhibit action potential generation and, thus, greatly affect nerve conduction and muscle contraction (Narahashi *et al.*, 1967). TTX and STX have guanidinium moieties (Lipkind & Fozzard, 1994) that are attracted to the negatively charged amino acids located in the ion selectivity filter of VGSCs (Catterall, 2000). Guanidinium is known to be positively charged at physiological pH, forming an electrostatic attraction with the channel (Lipkind & Fozzard, 1994). Both toxins are also stabilized by the formation of hydrogen bonds between their own hydroxyl and oxygen groups found within the pore (Kao & Walker, 1982). Yet, TTX and STX are too large to pass

through the channel, and therefore, physically occlude the outer pore, preventing ion flow (Narahashi, 2008). This block, however, does not affect channel gating, meaning the channel responds to a depolarizing stimulus in the same manor it would if TTX or STX were not present (Bezanilla & Armstrong, 1974).

### VGSC Enhancer: *Anemonia sulcata* Toxin II

*Anemonia sulcata* toxin II (ATX II) is a marine-based polypeptide known to increase the action potential duration in mammalian cardiac muscle preparations (Ravens, 1976). More specifically, low dose ATX II (2-20 nM) promoted an increased action potential duration without any significant change to resting membrane potential, and high dose ATX II (40 nM or greater) induced afterdepolarizations and triggered automaticity (Isenberg & Ravens, 1984). Both of these effects were inhibited by application of 60 μM TTX (Isenberg & Ravens, 1984). It was therefore believed that ATX II "modifies" sodium channels to induce a prolonged action potential duration (Isenberg & Ravens, 1984). Using electrophysiological techniques, it was proven that ATX-II effectively slows VGSC inactivation (Narahashi *et al.*, 1969), causes a positive shift in the voltage-dependence of inactivation (Murayama *et al.*, 1972) and actually has a voltage-dependence of binding (-60 mV or more positive; Isenberg & Ravens, 1984). It is commonly known that -60 mV is around the activation threshold of sodium channels (Catterall, 1979). Thus, this voltage-dependence implies that ATX II slows inactivation by interfering with the activation-inactivation coupling mechanism described earlier. Subsequent mutagenesis analysis identified a series of amino acids located on the S3-S4 extracellular loop in domain IV that were critical for toxin binding and action (Rogers *et al.*, 1996). Given that the S4 voltage sensor is responsible for activation (and activation-inactivation coupling), Rogers *et al.* (1996) proposed that ATX II slows channel inactivation by preventing the outward movement of the S4 transmembrane segment in

D4, thus preventing the required conformational changes necessary for fast inactivation to occur. This mechanism became known as the "voltage-sensor trapping mechanism" and is shared with several other polypeptide toxins (Rogers *et al.*, 1996; Cestele *et al.*, 1998; Cestele *et al.*, 2001).

## Transient and Persistent Sodium Current

The electrical activity of the heart and cardiac muscle cell contraction is dependent on a delicate balance of ion channels opening and closing, which allows the entry of sodium ($Na^+$) and calcium ($Ca^{2+}$), and the entry and exit of potassium ($K^+$). Sodium current ($I_{Na}$) is responsible for the very rapid depolarization of myocytes. As mentioned previously, sodium channels exist in three states: open, inactivated and closed (Catterall, 2000). Typically, $I_{Na}$ activates and inactivates very quickly (1-5 ms) and is followed by a recovery phase, which allows the channel to return to its resting state. This is known as transient sodium current ($I_{Na(T)}$) (Reviewed in Saint, 2008). Conversely, many types of excitable cells, including cardiac myocytes, possess a non-inactivating or slowly inactivating sodium current ($\geq$ 50 ms), known as persistent sodium current ($I_{Na(P)}$) (Reviewed in Saint, 2008). $I_{Na(P)}$ also differs from $I_{Na(T)}$ in its voltage-dependence of inactivation. In rat ventricular myocytes, $I_{Na(P)}$ had a $V_{50}$ (voltage of half maximal inactivation) nearly 20 mV more negative than $I_{Na(T)}$ (-52 mV for $I_{Na(P)}$ and -34 mV for $I_{Na(T)}$) (Saint *et al.*, 1992). By comparing peak currents, Saint *et al*. (1992) observed that $I_{Na(P)}$ was very small and accounted for only 1-2% of total current when compared to $I_{Na(T)}$ in native, healthy, myocytes. Although peak $I_{Na(P)}$ appears minimal in comparison to peak $I_{Na(T)}$, $I_{Na(P)}$ could theoretically pass an equal amount of sodium ions as $I_{Na(T)}$, as $I_{Na(P)}$ is non-inactivating (Reviewed in Saint, 2008). The effectiveness of $I_{Na(P)}$ can easily be seen in neocortical neurons, where $I_{Na(P)}$ accounts for only 0.25% of the total $I_{Na}$, yet, was modeled to be able to depolarize a neocortical pyramidal cell by 26 mV from a

resting potential of -50 mV (Alzheimer *et al.*, 1993). This suggests that although $I_{Na(P)}$ can be quite small, it can greatly affect membrane potential.

In the nervous system, $I_{Na(P)}$ serves many important functions such as synaptic transmission, neuronal plasticity and neuronal modulation (Crill, 1996). $I_{Na(P)}$ has been identified in mammalian neurons located in the cerebellum (Llinas & Sugimori, 1980), thalamus (Jahnsen & Llinas, 1984), hippocampus (French *et al.*, 1990), and neocortex (Amitai, 1994). In cardiomyocytes, however, the physiological role of $I_{Na(P)}$ is unknown. Previous experiments identified that blockade of $I_{Na(P)}$ significantly affected action potential amplitude and voltage rate of change, while leaving action potential duration, and more importantly, the excitation-contraction (E-C) coupling mechanism, unaffected (Brette & Orchard, 2006). Under normal physiological conditions, cardiac myocytes initiate an action potential when directed by a pacemaker cell, therefore, the idea that a cardiomyocyte could self-activate is highly unusual. Brette & Orchard (2006) hypothesized that $I_{Na(P)}$ may exist to act as a back-up mechanism that activates under pathological conditions (such as a depolarized resting membrane potential), though this theory has yet to be proven.

Several theories attempting to further elucidate $I_{Na(P)}$ have been postulated over the years. The first and original hypothesis was based on the concept of 'window' current. Window current is a phenomenon of ion channels in which inactivation does not have to occur, and thus channels can be persistently open (Attwell *et al.*, 1979). Window current is determined by plotting the activation and inactivation curves of an ion channel on the same graph. At some voltage, these two curves intersect and the area under the intersection is a region of voltages (typically -50 mV to -5 mV in cardiac myocyte) that form the window current voltage range (Bhatnagar *et al.*, 1990). The hypothesis of window current was later rejected once it was proven that $I_{Na(P)}$ could be

recorded essentially unchanged in magnitude at positive potentials; potentials far outside those predicted by window current (Saint *et al.*, 1992). Another feature distinguishing $I_{Na(P)}$ from window current is that $I_{Na(P)}$ will slowly inactivate overtime, whereas window current would theoretically be constant once fast inactivation has reached steady state (Noble & Noble, 2006). These characteristics suggest that window current can only account for a portion of $I_{Na(P)}$, facilitating the need for further explanation.

The second hypothesis regarding $I_{Na(P)}$ was that a single VGSC isoform could undergo multiple gating modes. This idea was supported by an experiment conducted by Fearon & Brown (2004), where they proved that a single VGSC isoform (recombinant $Na_V1.5$ expressed in HEK293 cells) could give rise to both $I_{Na(T)}$ and $I_{Na(P)}$. Moreover, it was observed that burst openings or non-inactivating currents occurred spontaneously in rat ventricular myocytes (Patlak & Ortiz, 1985). Patlak & Ortiz (1985) also demonstrated that $I_{Na(T)}$ and $I_{Na(P)}$ have the same conductance, TTX sensitivity (at micromolar concentrations) and sensitivity to holding potentials. They concluded that a single VGSC isoform could move slowly through several 'modes' of gating. However, it is now known that $I_{Na(P)}$ can be nearly eliminated by nanomolar concentrations of TTX whereas $I_{Na(T)}$ is unaffected by this concentration (Saint *et al.*, 1992). Although Patlak & Ortiz (1985) were incorrect about $I_{Na(T)}$ and $I_{Na(P)}$ having the same TTX sensitivity, their theory is still possible because it is known that different kinetic modes of VGSCs have different blocking affinities (Josephson & Sperelakis, 1989). Thus, a channel that stays in 'open' mode longer could have a higher affinity for TTX than a channel that inactivates rapidly.

Finally, the third hypothesis suggested that multiple sodium channel isoforms were present in the heart and specific isoforms contributed to $I_{Na(P}$ (Reviewed in Saint, 2008). This was supported by recent work indicating that mRNA transcripts for $Na_v1.1$, $Na_v1.2$ and $Na_v1.3$ and

$Na_v1.5$ were present in cardiac tissue (Haufe *et al.*, 2005). It was later identified that the dominant isoforms present in the heart are $Na_v1.5$ and $Na_v1.1$ (Reviewed in Saint, 2008).

**$Na_V1.5$**

$Na_v1.5$ is considered the dominant sodium channel isoform in the heart, being identified in large numbers at the intercalated discs of ventricular myocytes (Maier *et al.*, 2004). By localizing at the cell-to-cell junctions in ventricular myocytes, $Na_v1.5$ is therefore very important in the initiation and propagation of an action potential across the surface of the heart (Maier *et al.*, 2004). The genes for the α subunit of this sodium channel are located at 3p21-24 (Catterall *et al.*, 2005), and it is often paired with associating β1 and β3 subunits (Fahmi *et al.*, 2001).

**$Na_V1.1$**

$Na_v1.1$ has traditionally been considered a central nervous system (CNS) sodium channel, but it is now generally accepted that it is also located in cardiac muscle tissue. More specifically, the $Na_v1.1$ protein has been identified in the sinoatrial (SA) node of newborn rabbits (Baruscotti *et al.*, 1997) and in ventricular myocytes of mature mice and rats (Dhar Malhotra *et al.*, 2001). Further research into cardiac $Na_v1.1$ revealed that it exists in large numbers at the t-tubules of ventricular myocytes, even though it only contributes up to 5% of the total current recorded under whole-cell voltage-clamp (Maier *et al.*, 2002). The localization of $Na_V1.1$ indicates that it has a significant role in coupling the cell surface depolarization to a muscle contraction (Maier *et al.*, 2002).

**$Na_V1.1$ and $Na_V1.5$: Structural and Functional Differences**

Although $Na_v1.1$ and $Na_v1.5$ belong to the same family of ion channels, they have many distinct structural and functional properties. Pharmacologically, $Na_v1.1$ is often referred to as

TTX-sensitive and $Na_v1.5$ as TTX-resistant due to the fact that only nanomolar concentrations of TTX were required to block $Na_v1.1$ current, whereas $Na_v1.5$ current is blocked by micromolar concentrations of TTX (Frelin *et al.*, 1986). An inverse relationship between these two isoforms was observed using zinc or cadmium block (Frelin *et al.*, 1986). These differences in pharmacological sensitivities result from a single amino acid substitution in the outer pore of the channel (Heinemann *et al.*, 1992a). Mutational analysis identified that substituting F385 of D1 in neuronal sodium channels to the cysteine (C) 385 observed in cardiac sodium channels caused a substantial decrease in TTX/STX sensitivity, and a significant increase in zinc/cadmium sensitivity (Heinemann *et al.*, 1992a). This mutation substantially altered the effectiveness of TTX given that a strong hydrophobic interaction between a non-polar region of TTX and a tyrosine/phenylalanine residue (at position 385) was required to stabilize the toxin in the outer pore (Lipkind & Fozzard, 1994). The polar cysteine residue found in cardiac sodium channels interacted quite weakly with this non-polar region of TTX and thus formed a weak bond with the toxin (Lipkind & Fozzard, 1994).

Electrophysiologically, $Na_v1.1$ and $Na_v1.5$ have very different gating characteristics. $Na_v1.5$ is known to activate, inactivate and recover slower compared to $Na_v1.1$, as well as have a more negative range for voltage gating (Fozzard & Hanck, 1996). In regards to $I_{Na(P)}$, native $Na_v1.5$ inactivates very quickly and is unlikely to participate in burst openings or persistent current (Dumaine *et al.*, 1996). However, mutations in $Na_v1.5$, such as those seen in Long-QT syndrome, demonstrate persistent current with burst openings (Dumaine *et al.*, 1996). On the other hand, native $Na_v1.1$ is known to enter a $I_{Na(P)}$ gating mode. This was shown in cerebellar Purkinje neurons, where $Na_v1.1$ was deemed essential for the induction of $I_{Na(P)}$ and the generation sustained action potentials post stimuli (Kalume *et al.*, 2007). This claim was further

substantiated in $Na_v1.1$ knock out Purkinje neurons, where $I_{Na(P)}$ and $I_{Na(T)}$ were reduced by over 50% compared to $Na_v1.1$ positive Purkinje neurons (Kalume *et al.*, 2007). It should be noted that the knockout animals suffered from severe ataxia/seizures and died 15 days after parturition (Kalume *et al.*, 2007), indicating a vital role for $Na_v1.1$ and $I_{Na(P)}$ in the CNS.

## Hypoxia and Oxidative Stress

$I_{Na(P)}$ in the heart becomes particularly interesting during hypoxia and oxidative stress, because both conditions have been shown to exacerbate $I_{Na(P)}$. Hypoxia is induced in cardiac tissue primarily under two conditions: ischemia and myocardial infarction (MI). Both ischemia and MI reduce blood flow and result in less oxygen/nutrients being delivered to cardiac myocytes. Hypoxia is known to cause sodium loading in cardiac myocytes (Pike *et al.*, 1990). This can be attenuated by low concentrations of TTX, suggesting that sodium loading is a result of a non-inactivating, TTX-sensitive $I_{Na(P)}$ (Haigney *et al.*, 1994). Later studies using patch-clamp techniques revealed that hypoxia potentiates non-inactivating, TTX-sensitive $I_{Na(P)}$ (Ju *et al.*, 1996). Hypoxia specifically increased the frequency and amplitude of $I_{Na(P)}$ (Ju *et al.*, 1996). Ju *et al.* hypothesized that a PKC-dependent mechanism was inducing $I_{Na(P)}$. This stems from the fact that hypoxia increases the synthesis of phosphatidylserine, a compound which is necessary for PKC activity (Mozzi *et al.*, 1993). Therefore, Ju *et al.* (1996) concluded that increased phosphatidylserine would result in increased PKC activity, which in turn caused PKC to phosphorylate the inactivation gate of VGSCs, inhibiting the activity of the gate. Consequently, this would inhibit fast inactivation and promote a persistent current, leading to sodium loading in cells.

Ischemia-reperfusion (IR) injury commonly occurs during most ischemic or infarct events and is known to cause oxidative stress in the heart, leading to cardiac arrhythmias.

Ischemia results in decreased production of oxidative protective enzymes, as well as increased production of reactive oxygen species (ROS) which is exacerbated upon blood reperfusion (Ferrari *et al.*, 2004). Previous studies have identified that superoxide anions, hydroxyl radicals and hydrogen peroxide ($H_2O_2$) are produced during ischemia-reperfusion events (Zweier *et al.*, 1987). Initial studies conducted on frog ventricular myocytes illustrated that oxidative injury caused a slowing of inactivation as well as a positive voltage shift in inactivation and a negative voltage shift in activation (producing a larger 'window' current; Bhatnagar *et al.*, 1990). This finding was further substantiated in a later study where $H_2O_2$ caused a prolongation of action potential duration, which was inhibited by low concentrations of TTX (Ward & Giles, 1997). This study suggested that the prolonged action potential duration was a result of TTX-sensitive $I_{Na(P)}$. Interestingly, Ward & Giles (1997) identified that $I_{Na(P)}$ was only present using a perforated patch method, implying that intracellular messengers were the likely cause of the oxidative free radical-induced $I_{Na(P)}$. Several previous studies have demonstrated that $H_2O_2$ can indirectly activate PKC (Shasby *et al.*, 1988; Palumbo *et al.*, 1992; Natarajan *et al.*, 1993) and that PKC could be responsible for the cellular changes associated with oxidative injury (Ward & Moffat, 1995). The link between PKC and oxidative free radical-induced $I_{Na(P)}$ was demonstrated by Ward & Giles (1997), where they illustrated that inhibition of PKC resulted in a significant attenuation of action potential prolongation and thus the $I_{Na(P)}$ induced by $H_2O_2$ injury. It was also speculated that PKC would phosphorylate the inactivation gate of VGSCs, thereby inhibiting its function and promoting sodium loading in cardiac cells.

## Cardiac Arrhythmias

As was mentioned above, hypoxia and oxidative stress both exacerbate $I_{Na(P)}$ and promote sodium loading in cells. This sodium loading is believed to be the foundation of $I_{Na(P)}$ based

cardiac arrhythmias. The first arrhythmia observed from sodium loading is known as an early afterdepolarization (EAD). EADs occur in the middle of repolarization, are believed to have a sodium-dependent mechanism because they can be attenuated by TTX application (Song *et al.*, 2008), and are considered a result of failed repolarization (Noble & Noble, 2006). The exact mechanism of action that causes an EAD is still in question. The second arrhythmia observed from sodium loading is called a delayed afterdepolarization (DAD). DADs occur once repolarization is complete and are believed to occur via a calcium-based mechanism (Song *et al.*, 2008). Both of these arrhythmias can activate further depolarizing currents and if the stimulus is strong enough, result in automatic, repetitive action potentials (Song *et al.*, 2008).

Mechanistically, sodium loading in myocytes is believed to promote cellular calcium overload (Fraser *et al.*, 2006). This occurs via reactivation of calcium channels (Sipido *et al.*, 1995) or inhibition/reversal of the sodium-calcium exchanger (NCX) (Noble & Noble, 2006). Both situations result in further calcium release from intracellular stores, creating a significant calcium induced calcium release (Noble & Noble, 2006). This produces a transient inward current that is believed to be the foundation of DADs (Lederer & Tsien, 1976). As expected, blockade via TTX can eliminate both EADs and DADs, however, decreasing intracellular calcium using chelators, NCX inhibitors or intracellular calcium release blockers only inhibited DAD's (Song *et al.*, 2008).

$I_{Na(P)}$ based cardiac arrhythmias can also arise from a genetic mutation. Mutations to the SCN5A gene (coding the $Na_v1.5$ protein) have been known to induce an autosomal dominant disease known as Long Q-T Type 3 (LQT3; Sarkozy & Brugada, 2005). This disease is a specific type of congenital Long Q-T Syndrome, which is defined as a prolongation of the Q-T wave interval on an ECG, causing ventricular arrhythmias and potentially cardiac arrest and/or sudden

cardiac death (Sarkozy & Brugada, 2005). LQT3 is believed to arise via an inability of sodium channels to inactivate, which can result from channel re-openings post-stimulus (Bennett *et al.*, 1995) or deletion mutations at the areas important for inactivation (Wang *et al.*, 1995). A distinctive characteristic of LQT3 is that it occurs most often during sleep or rest, and rarely during exercise (Schwartz *et al.*, 2001). This gives rise to the possibility that LQT3 mutations allow $Na_v1.5$ to enter a $I_{Na(P)}$ gating mode activated by some oxidative stress. Oxidative stress can occur during sleep, and the most common inducer of oxidative stress is sleep apnea. Sleep apnea is defined as a chronic ailment caused by partial or complete collapse of the upper airway during rest and causes oxygen desaturation and hypoxia (Bentivoglio *et al.*, 2008); potentially inducing $Na_v1.5$ $I_{Na(P)}$ mortality seen in LQT3.

# Chapter 2

## Hypothesis and Objectives

The literature review presented above demonstrates the incredibly complex structure, function and pathologies of VGSCs in the heart. Most relevant to this project is that wildtype $Na_v1.1$, and not wildtype $Na_v1.5$, is likely responsible for the pathological $I_{Na(P)}$ observed during an oxidative challenge. I wish to prove this claim by directly testing the gating properties of native cardiac ventricular myocyte $I_{Na}$ and $Na_v1.5$ expressed in a mammalian cell line. I believe that by comparing the biophysical and pharmacological characteristics of native $I_{Na}$ to $Na_v1.5$, I can determine not only the gating characteristics of $Na_v1.5$, but also the likelihood that $Na_v1.1$ can affect cardiac ventricular myocyte function. **I hypothesize that $Na_v1.5$ is not responsible for the persistent current seen during an oxidative challenge**.

In order to test this hypothesis, I used freshly-dissociated right ventricular myocytes from male Sprague Dawley rats and HEK293 cells transiently-transfected with α-$Na_v1.5$. Using these models, I was able to successfully characterize the electrophysiological characteristics of native myocytes sodium current and isolated α-$Na_v1.5$ sodium current. Specifically, I used macro cell-attached voltage-clamp so that the decay of current (and thus inactivation) could be observed in the intact and unaltered cell. This patch clamp technique allowed me to satisfy the objectives of the experiment, which were:

1) Compare and contrast the biophysical properties of transiently-transfected HEK293 cells with α-$Na_v1.5$ to native cardiac ventricular myocytes $I_{Na}$

2) Compare and contrast the cellular responses of transiently-transfected HEK293 cells with α-$Na_v1.5$ to native cardiac ventricular myocytes $I_{Na}$ under the sodium channel enhancer ATX-II
3) Compare and contrast the cellular responses of transiently-transfected HEK293 cells with α-$Na_v1.5$ to native cardiac ventricular myocytes $I_{Na}$ under an ROS challenge.
4) Reverse the effect of the ROS challenge using low-dose TTX if the effect is present in transiently-transfected HEK293 cells with α-$Na_v1.5$ or native cardiac ventricular myocytes $I_{Na}$.

# Chapter 3

# Methods

## Cloned $Na_V1.5$

Previously in the lab, $Na_v1.5$ was cloned from adult rat ventricular myocytes and placed into a bicistronic vector (pcDNA3.1/V5-HisB- $Na_v1.5$ –IRES-GFP). This DNA was transformed into *Escherichia coli DH5*$\alpha$, and then extracted and purified using a Qiagen Plasmid Maxi/Mini Kit (Qiagen, Mississauga). This vector expressed both $Na_v1.5$ and green fluorescent protein (GFP), thus a successfully transfected cell was easily identified via a bright, green glow under blue light (excites at approximately 400 nm, emits at approximately 500 nm).

## HEK293 Cell Culture

HEK293 cells (American Type Culture Collection, Rockville, MD) were seeded in 60 mm-diameter Petri dishes and grown in Dulbecco's Modified Eagle Medium (DMEM)/high glucose (4500 mg/L) with L-Glutamine (4.00 mM) (ThermoScientific, Rockford, IL) and with 10% Fetal Bovine Serum (FBS) (Invitrogen, Carlsbad, CA). Cells were passaged every 4 days via trypsinization to promote new cell growth and cells became one generation older each time passaged. Cells were deemed viable from generation 3 to approximately generation 40, pending growth rates and a minimum 25% transfection rate.

## HEK293 Transfection with $Na_V1.5$

The cloned $Na_v1.5$ channel was transfected into HEK293 cells using 10 μL of Lipofectamine 2000 (Invitrogen, Carlsbad, CA) and 4 μg of $Na_v1.5$-DNA. Cells were transfected in 35 mm-diameter Petri dishes containing Opti-MEM Reduced Serum Media (with HEPES and

sodium bicarbonate, hypoxanthine, thymidine, sodium pyruvate, L-glutamine, trace elements and growth factors) (Invitrogen, Carlsbad, CA). After 40 hours, approximately 50-70% of cells fluoresce green, indicating GFP expression in the cytoplasm. Cells were harvested via trypsinization, immediately placed in DMEM with 10% FBS, and pipetted onto several 8 mm cover slips. Once pipetted, cells were incubated for 60 minutes at 37 °C and were deemed viable up to 5 hours post trypsinization.

## Cardiac Myocyte Isolation

All experimental protocols that required animals were approved by the Queen's University Animal Care Committee following the principles established by the Canadian Council on Animal Care. Male Sprague Dawley rats (225-250 g, Charles River) were humanely decapitated and their hearts rapidly harvested and mounted on a cannula for perfusion at a rate of approximately 10 mL/min using a standard Langendorff apparatus. Hearts were immediately perfused for 5 minutes with a Tyrodes solution (composition, mM: NaCl 140; KCl 5.4; $MgCl_2$ 1; $Na_2HPO_4$ 1; HEPES 5; glucose 10; $CaCl_2$ 1; pH 7.4 using NaOH). Hearts were next perfused for 5 minutes using $Ca^{2+}$-free Tyrodes and finally for 8 minutes using modified Tyrodes; to which $CaCl_2$ (0.04 mM), collagenase (0.02 mg/mL Type II, Yakult Co. Ltd, Tokyo), and protease (0.004 g/250 mL Type XIV, Sigma Aldrich) had been added. All solutions were constantly gassed with 100% $O_2$ and were warmed to 37 °C prior to perfusion.

Immediately following perfusion of modified Tyrodes, the right ventricle was dissected and minced in 5 mL of a second modified Tyrodes (compound, quantity; $CaCl_2$ 0.1 mM; collagenase 0.05 mg/mL (Type II, Yakult Co. Ltd, Tokyo); protease 0.1 g/ 250mL (Type XIV, Sigma Aldrich)). This solution was agitated in a reciprocal shaking bath (Thermoscientific, Rockford, IL) at 37 °C. Once individual myocytes could be observed (approximately 15 minutes),

cells were collected and aliquoted into 3 mL of Kraft-Brühe (KB) storage solution (composition, mM: potassium glutamate 100; potassium aspartate 10; KCl 25; glucose 20; $KH_2PO_4$ 10; HEPES 5; $MgSO_4$ 2; taurine 20; creatine 5; EGTA 0.5; BSA 1 mg/mL; pH 7.2 with KOH). Cells were aliquoted every 3 minutes, 6 times, for a total digestion time of approximately 30 minutes. Myocytes were stored in KB at 4 °C for a minimum of 60 minutes prior to use. Cells were viable for 5-6 hours after initial storage.

## Electrophysiological Methods

For my experiments, I used macro cell-attached voltage-clamp because $H_2O_2$-induced $I_{Na(P)}$ cannot be observed under whole-cell voltage-clamp (Barrington, 1994; Ward & Giles, 1997) and perforated voltage-clamp does not allow a low enough access resistance to accurately record $I_{Na}$. Previous experiments have demonstrated that macro cell-attached voltage-clamp is effective in examining myocyte $Na^+$ channel kinetics (Bodewei *et al.*, 1982; Benndorf *et al.*, 1985; Kunze *et al.*, 1985; Berman *et al.*, 1989; Murray *et al.*, 1990) and will allow us to study $I_{Na}$ in isolation for both HEK293 cells and native cardiac myocytes.

Cells were plated in the perfusion chamber of an inverted microscope (Nikon Eclipse TE2000s) and perfused using a gravity-based flow system (1-2 mL/min) containing a Tyrodes solution (composition, mM: NaCl 140; KCl 5.4; $Na_2HPO_4$ 1; $CaCl_2$ 1; $MgCl_2$ 1; HEPES 5; glucose 10, pH to 7.4 with NaOH). For myocytes, cells were plated and given 10 minutes to adhere to the chamber bottom prior to commencing flow. For all HEK293 cells, coverslips were perfused immediately and given 10 minutes to adjust to the Tyrodes solution. Fire-polished borosilicate glass pipettes (WPI, Sarasota, FL) were made using a microprocessor-controlled, multi-stage puller (P97, Sutter Instruments). The tips of the borosilicate pipettes were coated with Sylgard Silicone 184 Elastomer (Dow Corning, Michigan) and hot air dried using a hand held

electric heat gun. Coating the tips increased their overall size (thus, increasing the size of the capacitor), which increased the distance between electrolyte solutions and helped to control for changes in capacitance that create noise. Tips with resistances that fell between 1-2 MΩ were backfilled using an internal solution (composition, mM: NaCl 140; KCl 5.4; $Na_2HPO_4$ 1; $CaCl_2$ 1; $MgCl_2$ 1; HEPES 5; glucose 10, pH to 7.4 with NaOH). For myocytes, 0.1 mM $Ba^{2+}$ was added to the internal solution to suppress inwardly rectifying $K^+$ channels. All experiments were performed at room temperature (21 °C-22 °C).

Cells were selected for patch clamp based on a visual assessment of overall health. For myocytes, this implied a rectangular shape, vivid striations and smooth edges indicating an intact membrane. For non-transfected HEK293 cells, only a clear and spherical membrane was required. For transfected HEK293 cells, a bright green glow, combined with a clear and spherical membrane was necessary.

Current was recorded using a HEKA EPC 8 headstage attached to a HEKA patch clamp EPC 8 amplifier (HEKA Instruments, New York) and displayed on a computer using pClamp 10.0/Digidata 1440A software (Axon Instruments, USA). Data was sampled at 50 kHz (every 20 μs) and filtered at 7 kHz. To determine resistance, capacitance currents were elicited by 30 ms, 10 mV depolarizing pulses from a holding potential of -70 mV. All currents were corrected to pipette (fast) capacitance and amplified at a ratio of 20 mV/pA or 50 mV/pA to allow for visualization of the small currents.

**HEK293 Voltage-Clamp Protocols**

Initial tests of HEK293 cells (transfected and non-ttransfected) indicated that their resting membrane potentials (using perforated current-clamp) were approximately -20 mV. The nature of cell-attached voltage-clamp states that any voltage applied to a cell must be summated to the

resting membrane potential, and the resulting value is the true voltage in the cell. Also, because there is no membrane rupture in cell-attached voltage-clamp, hyperpolarizing voltages are applied to the outer cell membrane in order to induce a depolarization within the cytosol. Therefore, in order to obtain an assumed holding potential ($V_H$) of 160 mV; voltage clamp protocols added 140 mV to HEK293 cells. All voltage steps accounted for the resting membrane potential.

Current voltage (IV) relationships were obtained using 100 ms voltage steps, applied at 1 Hz, from an assumed holding potential of 160 mV to assumed command potentials of 90 mV, 80 mV, 70 mV and 60 mV (Figure 2A, B). Each potential was tested individually and 50 consecutive sweeps were recorded. Identically timed blank sweeps were recorded at voltages that did not activate any channels and were from an assumed holding potential of 100 mV to assumed command potentials of 30 mV, 20 mV, 10 mV and 0 mV (Figure 2C, D). Inactivation data was collected using 105 ms assumed command potentials of 160 mV, 140 mV and 120 mV followed by a 100 ms assumed test pulse of 80 mV to activate any available channels (Figure 3A, B). Identically timed blank sweeps were recorded from an assumed holding potential of 100 mV to assumed command potentials of 20 mV, 40 mV and 60 mV. (Figure 3C, D).

**Ventricular Myocyte Voltage-Clamp Protocols**

Ventricular myocytes were determined (using perforated current-clamp) to have a resting membrane potentials were approximately -80 mV. Thus, in order to obtain an assumed holding potential ($V_H$) of 160 mV; voltage clamp protocols added 80 mV to cardiac myocytes. All voltage steps accounted for the resting membrane potential.

IV relationships were obtained using 100 ms voltage steps, applied at 1 Hz, from an assumed holding potential of 160 mV to assumed command potentials of 80 mV, 70 mV, 60 mV and 50 mV. Each potential was tested individually and 50 sweeps were recorded per command

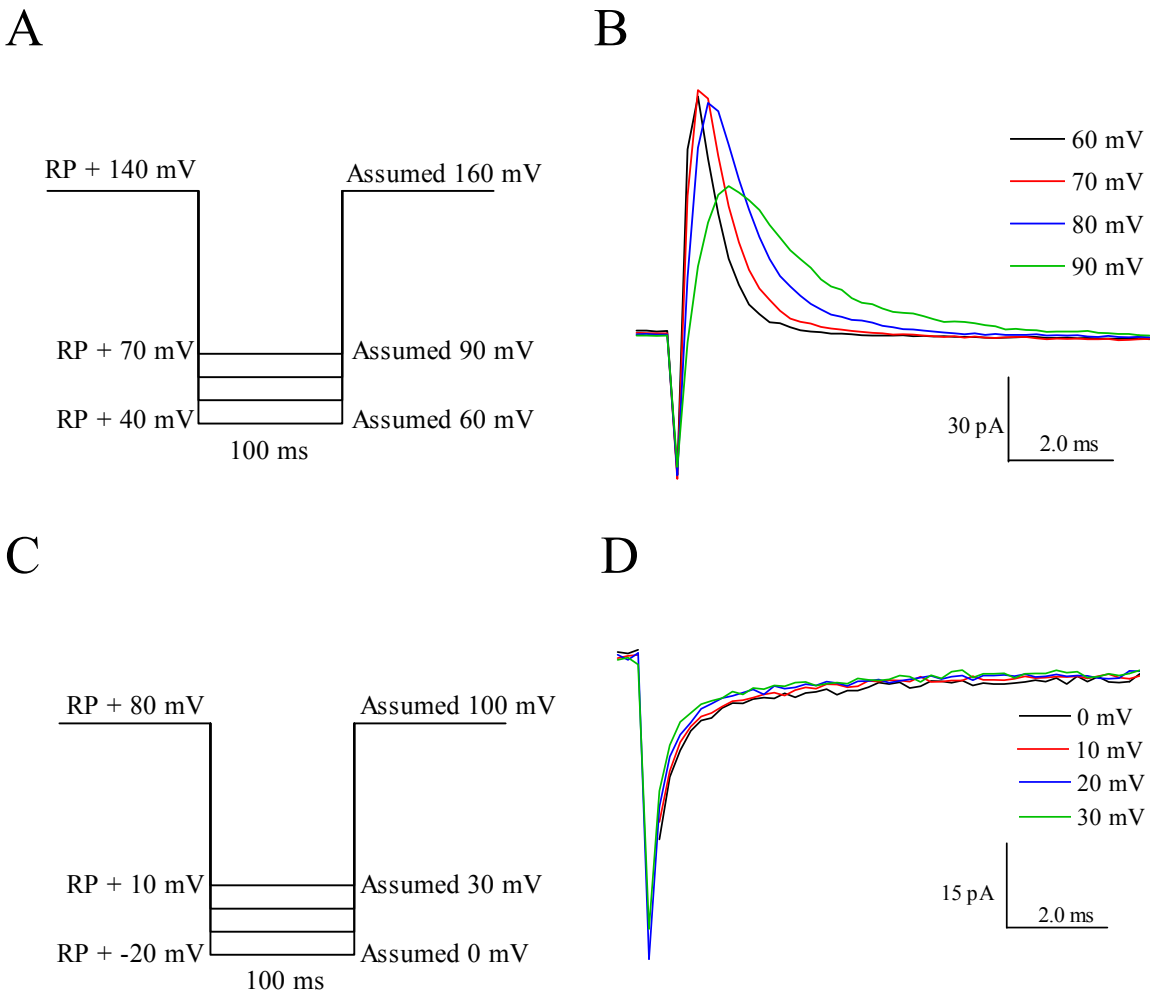


**Figure 2: $Na^+$ Channel Current–Voltage (IV) Relationship.** (A): HEK293- $Na_V1.5$ IV protocol with voltage steps from 160 mV to 90 mV, 80 mV, 70 mV and 60 mV. (B): Representative data illustrating $Na^+$ currents recorded using the protocol outlined in A. Note that each trace is an average of 50 consecutive sweeps. (C): HEK293- $Na_V1.5$ blank IV protocol with voltage steps from 100 mV to 30 mV, 20 mV, 10 mV and 0 mV. (D): Representative data illustrating sweeps devoid of $Na^+$ current recorded using the protocol outlined in B. Note that these traces were used for capacitance subtraction.

voltage. Identically timed blank sweeps were recorded from a holding potential of 100 mV to command potentials at 20 mV, 10 mV, 0 mV and -10 mV. Inactivation data was collected using 105 ms command potentials at 160 mV, 140 mV, 120 mV, 110 mV and 105 mV (if necessary) followed by a 100 ms test pulse to 50 mV to activate any available channels. Identically timed blank sweeps were recorded from a holding potential of 100 mV to command potentials at -10 mV, 10 mV, 30 mV, 40 mV and 45 mV (if necessary).

## Treatment Preparation and Application

For the macro cell-attached voltage-clamp method, all treatments were applied via the borosilicate pipette, which was filled with the treatment-containing internal solution. A maximum dilution of 1µL/mL was permitted to prevent any unwanted vehicle-based effects. The three treatments used were ATX II, TTX and $H_2O_2$ and prepared as follows.

- ATX II (100 µM; Sigma Aldrich) dissolved in $_{dd}H_2O$
- TTX (100 µM; Alomone Labs, Israel) dissolved in pure acetic acid
- $H_2O_2$ (1 M; Fisher Scientific) diluted using $_{dd}H_2O$

The final concentrations used in the experiments were selected in accordance with the literature. 10 nM ATX II was shown to potently enhance $Na_v1.5$ current in cardiac myocytes (Isenberg & Ravens, 1984). 10 nM TTX was the appropriate concentration to block $Na_v1.1$ (Heinemann *et al.*, 1992a) and $I_{Na(P)}$ (Ju *et al.*, 1996), while leaving $Na_v1.5$ unaffected (Heinemann *et al.*, 1992a). 100-200 µM $H_2O_2$ was within the concentration range that activates $I_{Na(P)}$ under perforated current- clamp (Ward & Giles, 1997).

Given the nature of macro cell attached patch, it is impossible to record control and treatment data from the same patch. Therefore, control and treatment data were recorded in

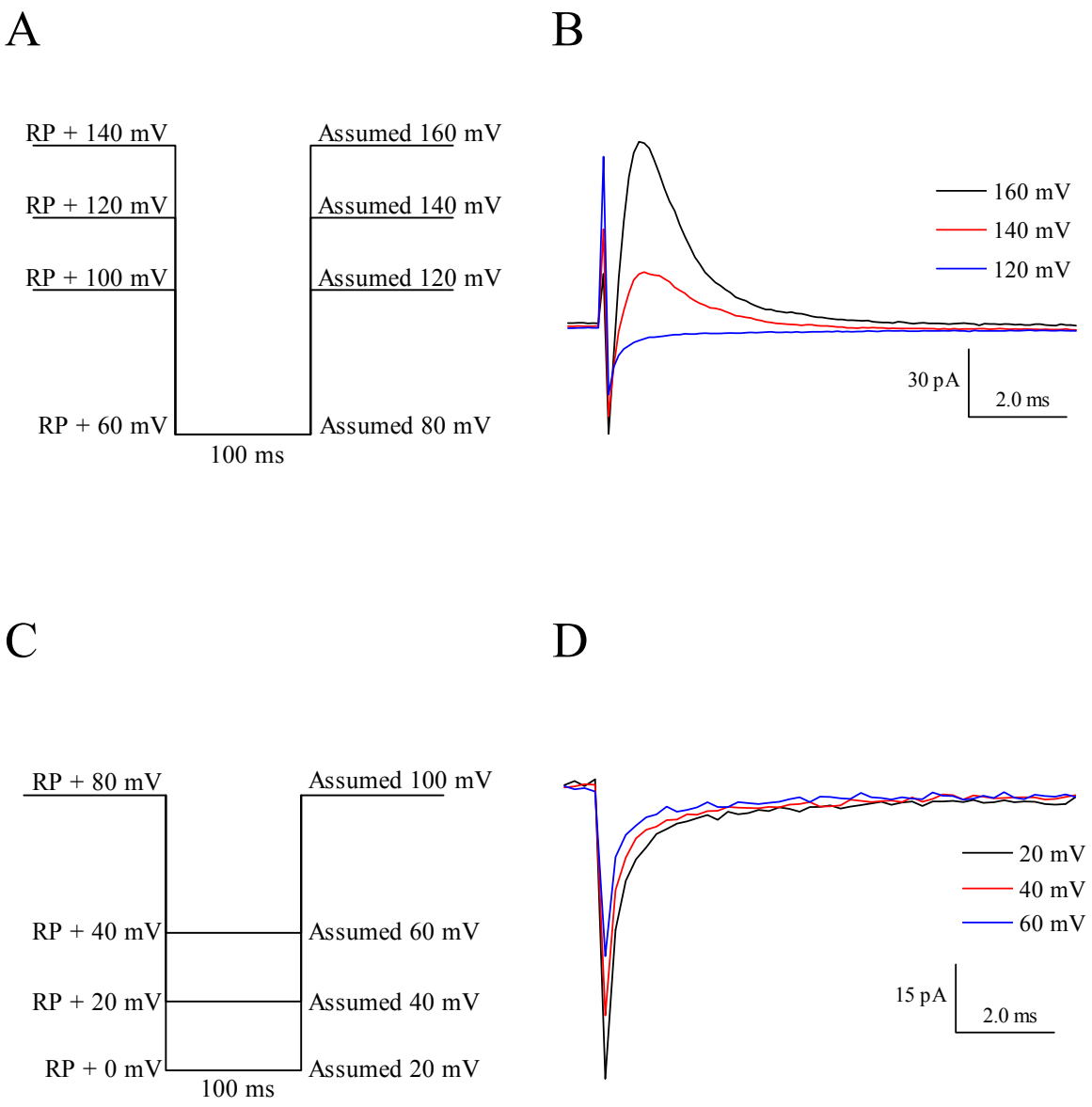


**Figure 3: $Na^+$ Channel Voltage-Dependence of Inactivation.** (A): HEK293- $Na_V1.5$ inactivation protocol with voltage steps from 160 mV, 140 mV and 120 mV to 80 mV. (B): Representative data illustrating $Na^+$ currents recorded using the protocol outlined in A. Note that each trace is an average of 50 consecutive sweeps. (C): HEK293- $Na_V1.5$ blank inactivation protocol with voltage steps from 100 mV to 60 mV, 40 mV and 20 mV. (D): Representative data illustrating sweeps devoid of $Na^+$ current recorded using the protocol outlined in B. Note that these traces were used for capacitance subtraction.

separate cells, and often on separate days. During treatments, 10 minutes was allotted to allow the compound to diffuse from the internals solution of the pipette to the surface of the cell.

## Data Analysis

Current from the protocols that elicited no channel activity were used to correct for capacitance transients, leakage current and present the current as inward. All currents and voltages in the results will be expressed as negative, as per convention. Ensemble currents were obtained by averaging 40-50 sweeps, giving an overall representation of current and decay for any given voltage. (Figure 4A, B). This is because in cell attached patch clamp, a hyperpolarizing voltage is delivered to the outside of the plasma membrane, and thus a depolarizing voltage would be observed at the inside of the plasma membrane.

For the IV and inactivation protocols, peak amplitude (pA), area under the curve (AUC; pA • ms), binomial exponential decay and half maximal inactivation ($V_{50}$) were extrapolated. The binomial decay gave two tau values, which were identified as 'fast tau' and 'slow tau' (Figure 4C). In order to account for varying number of channels in a given patch (and thus varying peak amplitude/area under the curve), area under the curve was normalized to peak amplitude such that the amount of relative AUC could be compared between cells and treatment trials. Area under the curve had to be normalized to peak amplitude because cell size (pF) is irrelevant to the amount of current recorded in cell-attached voltage-clamp and tip size (MΩ) does not account for varying channel densities between cells.

### Statistical Analysis

Results were expressed as means ± standard error of the mean (S.E.M). All data was determined to be nonparametric and therefore the tests primarily used were the Mann Whitney U-

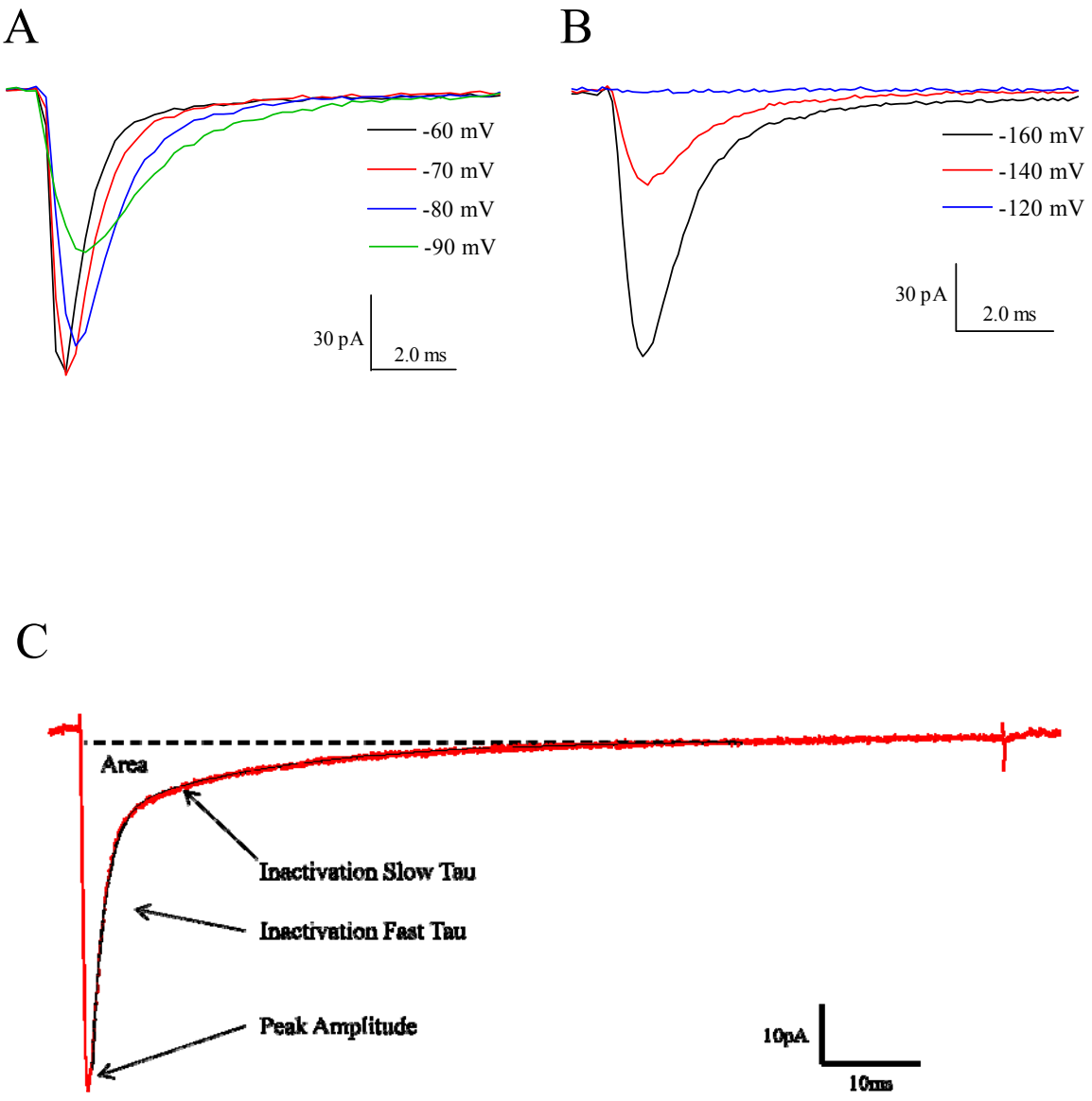


**Figure 4: $Na^+$ Channel Data Analysis.** (A): HEK293- $Na_V1.5$ transformed IV tracing with no capacitive currents and a conventional inward direction. (B): HEK293- $Na_V1.5$ transformed inactivation tracing with no capacitive currents and a conventional inward direction. (C): Sample trace identifying the data to be extrapolated from the results: area under the curve, inactivation decay fast tau, inactivation decay slow tau and peak current magnitude.

test when comparing two groups, and the Kruskal-Wallis (with Post-Dunn's test) when comparing three or more groups. Linear regression analysis was performed on select IV curves in order to determine significance from 0. A probability of $P < 0.05$ was considered statistically significant. Statistical analysis was performed using Graphpad Prism version 4.00.

# Chapter 4

# Results

## Non-Transfected and Transfected HEK293 cells Current-Voltage (IV) Relationships

The IV relationship of $Na_V1.5$ was assessed by expressing the channel in HEK293 cells. For transfected HEK293 cells (n=5), command voltages ($V_C$) of -60 mV, -70 mV, -80 mV and -90 mV resulted in inward currents of -62.4±14.6 pA, -50.6±16.1 pA, -31.2±16.0 pA, and -18.6±10.8 pA, respectively (Figure 5A), which were significantly different from baseline (0 pA; $P<0.05$). In contrast, non-transfected HEK293 cells (n=5), subjected to identical voltage protocols, possessed currents that were insignificantly different from 0 pA ($P<0.05$; Figure 5A). Thus, I observed no endogenous currents in my HEK293 cells, and all recorded currents from transfected HEK293 cells are purely $Na_V1.5$, with no contamination from other ion channels.

## Effects of ATX II and $H_2O_2$ on Transfected HEK293 cells

After determining that transfected HEK293 cells displayed inward current, I applied 10 nM ATX II to not only confirm that the current observed is from VGSCs, but to also show that the transfected cells can display persistent current. For other experiments, I then applied $H_2O_2$ at two concentrations, 1 mM and 100 μM, in an attempt to induce $I_{Na(P)}$. 1 mM is an extremely high concentration for $H_2O_2$ and was lethal to cardiac myocytes, but was added in HEK293 cells in an attempt to force $H_2O_2$-induced $I_{Na(P)}$.

## Effects of ATX II and $H_2O_2$ on the Current-Voltage Relationship in Transfected HEK293 cells

I initially examined any effects that 10 nM ATX II (n=3), 1 mM $H_2O_2$ (n=5) and 100 μM $H_2O_2$ (n=4) might exert on the control (n=5) IV relationship (Figure 5B; Table 1). Beginning with

control transfected HEK293 cells, command voltages ($V_C$) of -60 mV, -70 mV, -80 mV and -90 mV resulted in inward currents of -62.4±14.6 pA, -50.6±16.1 pA, -31.2±16.0 pA, and -18.6±10.8 pA, respectively. These currents were voltage-dependent, such that a smaller voltage step elicited a smaller current response, and this effect was conserved across all experimental groups. When examining the effects of 10 nM ATX II, I saw a non-significant increase in peak values across all voltages. An example of this is seen at the peak command voltage ($V_C$ -60 mV), where the resulting current was -76.2±25.5 pA, approximately 14 pA greater than control (Figure 5B; Table 1). When examining the effects of $H_2O_2$, I saw a pronounced concentration-dependent response. Specifically, 1 mM $H_2O_2$ induced currents that were less than control values at all voltages (Figure 5B; Table 1). This effect was most pronounced at $V_C$ -60mV, where recorded current was only -25.3±5.8 pA, approximately 38 pA less than control. At 100 µM $H_2O_2$, we saw current responses that were slightly greater across all voltages relative to control, although non-significant (Figure 5B; Table 1).

**Effects of ATX II and $H_2O_2$ on Normalized Area under the Curve in Transfected HEK293 cells**

Although there were no significant differences in peak current between control and any of the experimental groups, I nevertheless wanted to examine area under the curve. It would be expected that any effect inducing $I_{Na(P)}$ would be easily identified via area under the curve analysis. To directly test the effects on area under the curve, I normalized area under the curve to peak current amplitude for all cell types. This is because although peak amplitudes were not statistically significant, the data presented previously illustrates that there is variability among the peak amplitude values. Therefore, normalizing area under the curve to peak amplitude would remove some variability between the cell groups.

A

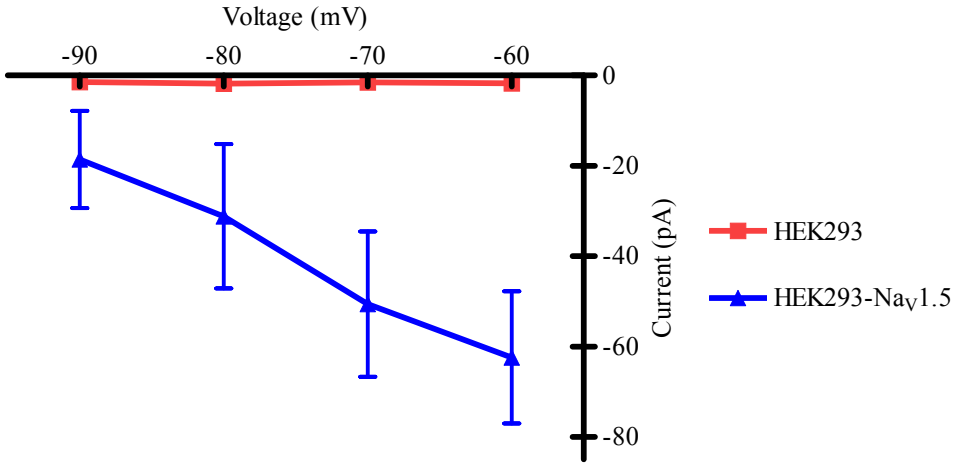


B

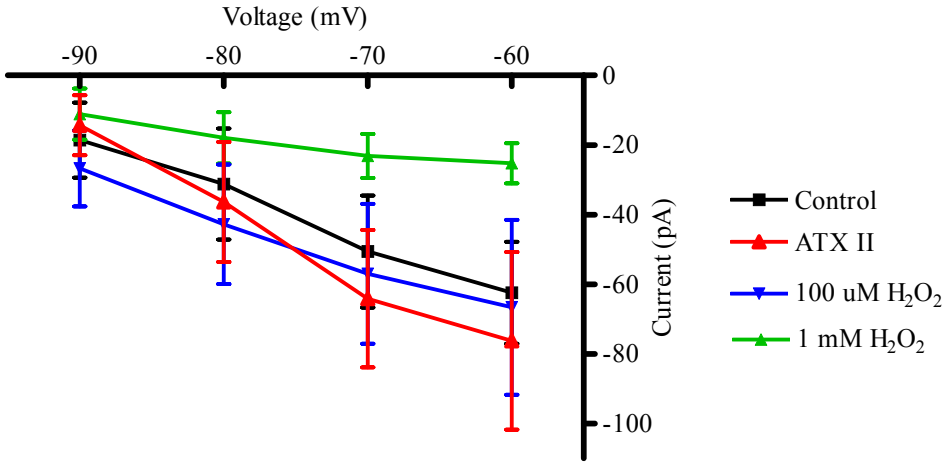


**Figure 5: Current-Voltage (IV) Relationships in HEK293 cells.** (A): Comparison of IV relationships for peak $I_{Na}$ between non-transfected HEK293 cells (n=5) and transfected HEK293 cells (n=5). Non-transfected HEK293 current is not different from 0 across all voltages (P>0.05). (B): Effects of 10 nM ATX II (n=3; red), 1 mM $H_2O_2$ (n=5; green) and 100 µM $H_2O_2$ (n=4; blue) on peak $I_{Na}$ relative to control (n=5; black) in transfected HEK293 cells. Values represent the mean ± standard error mean.

| Command Voltage ($V_C$) | Control | 10 nM ATX II | 1 mM $H_2O_2$ | 100 μM $H_2O_2$ |
|---|---|---|---|---|
| -60 mV | -62.4±14.6 pA | -76.2±25.5 pA | -25.3±5.8 pA | -66.6±25.1 pA |
| -70 mV | -50.6±16.1 pA | -64.1±19.7 pA | -23.2±6.3 pA | -56.9±20.1 pA |
| -80 mV | -31.2±16.0 pA | -36.4±17.3 pA | -18.0±7.4 pA | -42.8±17.1 pA |
| -90 mV | -18.6±10.8 pA | -14.4±8.6 pA | -11.1±7.3 pA | -26.7±10.9 pA |

**Table 1: Current-Voltage (IV) Relationship in Transfected HEK293 cells.** Effects of 10 nM ATX II (n=3), 1 mM $H_2O_2$ (n=5) and 100 μM $H_2O_2$ (n=4) on peak $I_{Na}$ relative to control (n=5) transfected HEK293 cells. Values represent the mean ± standard error mean.

When examining the effects of 10 nM ATX II (n=5), 1 mM $H_2O_2$ (n=5) and 100 μM $H_2O_2$ (n=4) on control (n=5) normalized area under the curve, there were some striking differences (Figure 6; Table 2). Starting with control transfected HEK293 cells, command voltages ($V_C$) of -60 mV, -70 mV, -80 mV and -90 mV resulted in normalized area under the curve values of -3.3±0.8 relative AUC, -4.7±1.1 relative AUC, -6.7±1.6 relative AUC, and -8.5±2.8 relative AUC, respectively. These values indicate that area under the curve exhibits voltage-dependence. However, contrasting the current-voltage (IV) relationship data, a smaller voltage step elicited more normalized area under the curve and this effect was not conserved across all experimental groups. Regarding the experimental groups, I saw that ATX II non-significantly increased normalized area under the curve across all voltages, while maintaining the voltage-dependent effect seen in control settings (Figure 6; Table 2). In regards to $H_2O_2$, I again saw a concentration-dependent effect of the compound. At the 1 mM concentration, I saw a non-significant increase in normalized area under the curve at $V_C$ -60 mV (Figure 6A), -70 mV (Figure 6B), and no effect relative to control at $V_C$ -80 mV (Figure 6C), -90 mV (Figure 6D). At this concentration, the voltage-dependent effect observed under a control environment is no longer present, indicating that 1 mM $H_2O_2$ has a pronounced effect on $Na^+$ channel kinetics. At the 100 μM concentration, I saw a non-significant decrease in normalized area under the curve at $V_C$ -70 mV (Figure 6B), -80 mV (Figure 6C) and -90 mV (Figure 6D), as well as a minor alteration in the voltage-dependence observed in control cells (Figure 6; Table 2). These effects, however, were not near as dramatic as those observed in 1 mM $H_2O_2$.

**Effects of ATX II and $H_2O_2$ on the Time-Dependence of Inactivation in Transfected HEK293 cells**

I next examined the effects of the treatment groups on the time-dependence of

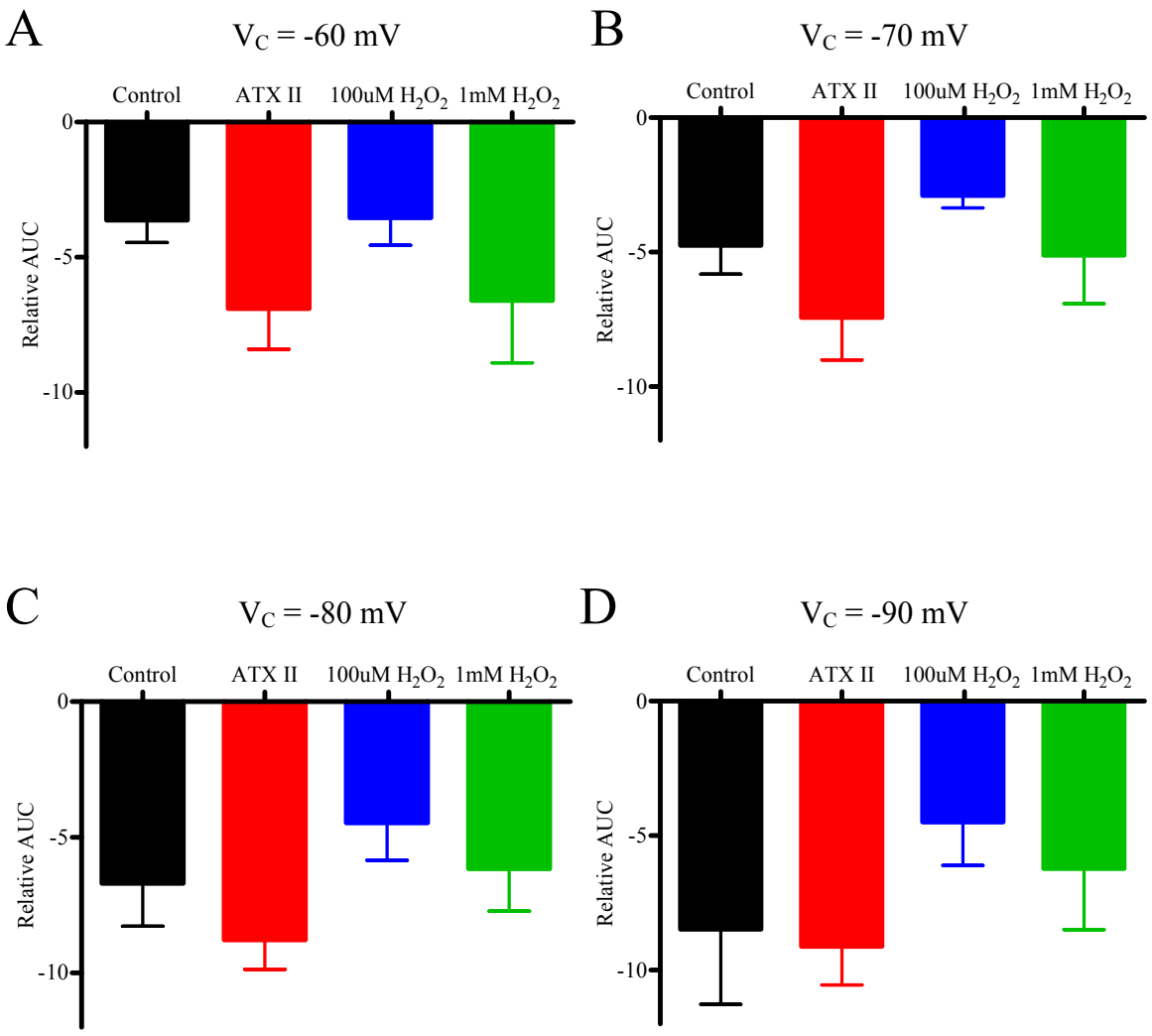


**Figure 6**: **Normalized Area under the Curve (AUC) in HEK293 cells.** Effects of 10 nM ATX II (n=5; red), 100 µM $H_2O_2$ (n=4; blue) and 1 mM $H_2O_2$ (n=5; green) on normalized area under the curve relative to control (n=5; black) in transfected HEK293 cells at the command voltage ($V_C$) -60 mV (A), $V_C$ -70 mV (B), $V_C$ -80 mV (C), and $V_C$ -90 mV (D). Values represent the mean ± standard error mean.

| Command Voltage ($V_C$) | Control | 10 nM ATX II | 1 mM $H_2O_2$ | 100 μM $H_2O_2$ |
|---|---|---|---|---|
| -60 mV | -3.3±0.8 | -6.9±1.5 | -6.6±2.3 | -3.5±1.0 |
| -70 mV | -4.7±1.1 | -7.4±1.6 | -5.1±1.8 | -2.9±0.5 |
| -80 mV | -6.7±1.6 | -8.8±1.1 | -6.2±1.6 | -4.5±1.4 |
| -90 mV | -8.5±2.8 | -9.1±1.4 | -6.2±2.3 | -4.5±1.6 |

**Table 2: Normalized Area under the Curve (AUC) in HEK293 cells.** Effects of 10 nM ATX II (n=5), 1 mM $H_2O_2$ (n=5) and 100 μM $H_2O_2$ (n=4) on normalized area under the curve relative to control (n=5) transfected HEK293 cells. Values are reported as relative AUC and represent the mean ± standard error mean.

inactivation as calculated as tau, the time it takes for 67% of the current to decay. It was expected that any effects that prolong inactivation would present themselves in the decay tau. As stated in the methods, the inactivation component (decay of the current) represented a binomial exponential decay and therefore two tau values were measured: fast tau and slow tau. I was only able to examine tau values for the three largest command voltages (-60 mV, -70 mV and -80 mV). Many current values at -90 mV were too close to 0 pA, and any variations in baseline caused dramatic changes in tau.

With regards to fast tau, the time constants under control parameters at $V_C$ -60 mV, -70 mV and -80 mV were 1.3±0.2 ms, 1.7±0.4 ms, and 2.6±0.8 ms, respectively (Figure 7A, C, E; Table 3A). These data depict an identical voltage-dependence to that observed in normalized area under the curve. Also, in regards to the experimental groups, the data for fast tau inactivation gives identical results to those seen in normalized area under the curve. I saw the same loss of voltage-dependence in the $H_2O_2$ groups as well as the same non-significant value increase in 10nM ATX II and 1mM $H_2O_2$ relative to control (Figure 7A, C, E; Table 3A). Therefore, it appears that fast tau decay greatly influences normalized area under the curve, and thus the amount of charge that an ion channel can pass.

Regarding slow tau, the time constants under control settings at command voltages ($V_C$) -60 mV, -70 mV, and -80 mV were 18.5±2.8 ms, 16.0±4.0 ms, and 20.2±6.4 ms, respectively (Figure 7B, D, F; Table 3B). As can be seen from this data, there is no voltage- dependence, and thus, slow tau appears to be constant throughout this IV relationship. This trend, however, was not observed in any of the experimental groups. 10 nM ATX II followed a non-significant voltage-dependent trend, such that as voltage steps became smaller, the time course of slow tau increased (Figure 7B, D, F; Table 3B). This effect was also observed in both fast tau inactivation

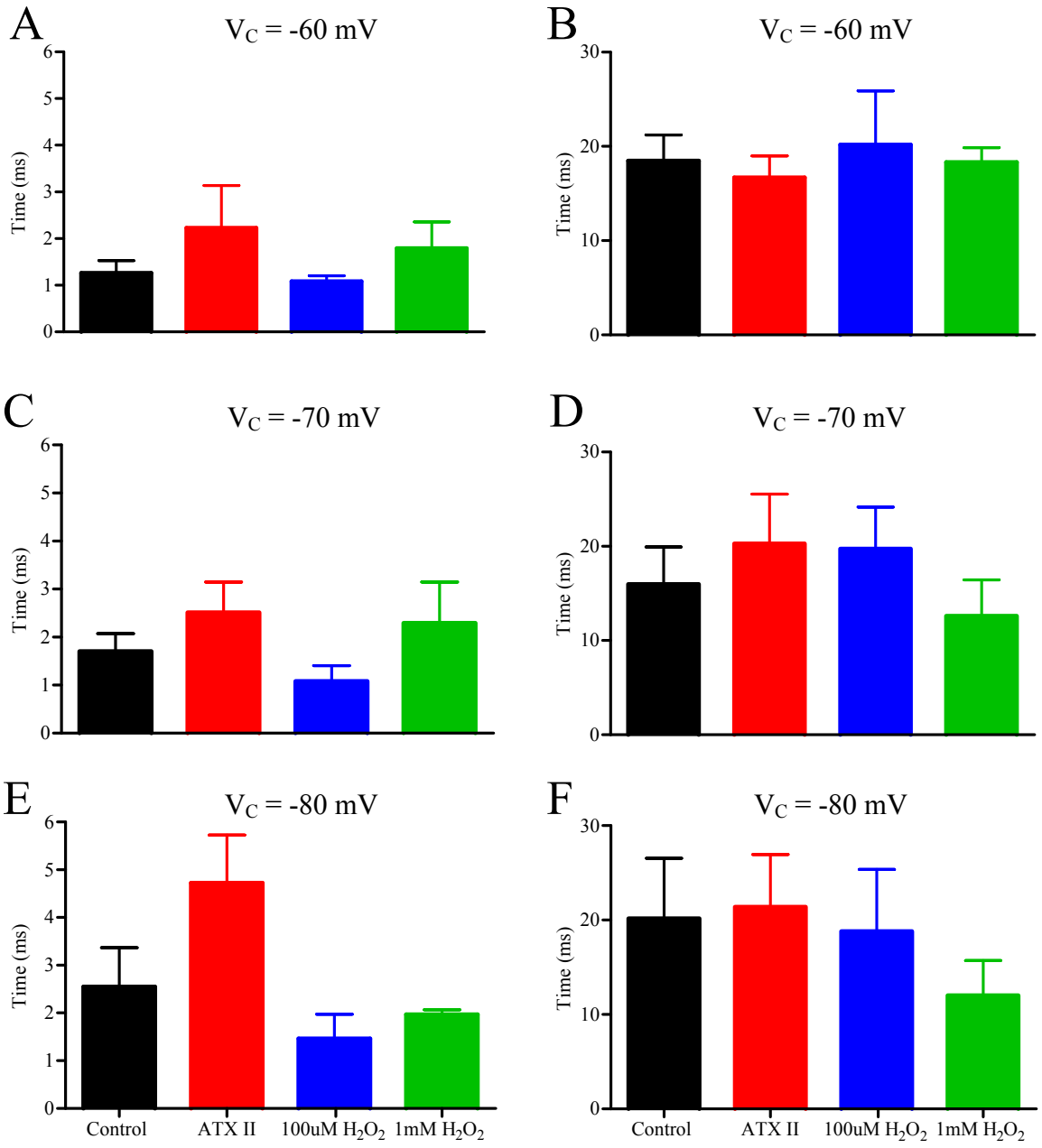


**Figure 7**: **Effects on Inactivation in HEK293 cells.** Effects of 10 nM ATX II (red), 100 µM $H_2O_2$ (blue) and 1 mM $H_2O_2$ (green) on fast tau decay (inactivation) relative to control (black) in transfected HEK293 cells at the command voltage ($V_C$) -60 mV (A), $V_C$ -70 mV (C) and $V_C$ -80 mV (E). Effects of 10 nM ATX II (n=5; red), 100 µM $H_2O_2$ (n=4; blue) and 1 mM $H_2O_2$ (n=5; green) on slow tau decay (inactivation) relative to control (n=5; black) in transfected HEK293 cells at the command voltage ($V_C$) -60 mV (B), $V_C$ -70 mV (D), and $V_C$ -80 mV (F). Values represent the mean ± standard error mean.

A

| Fast Tau | | | | |
|---|---|---|---|---|
| Command Voltage ($V_C$) | Control | 10 nM ATX II | 1 mM $H_2O_2$ | 100 μM $H_2O_2$ |
| -60 mV | 1.3±0.2 ms (n=5) | 2.2±0.9 ms (n=5) | 1.8±0.6 ms (n=5) | 1.1±0.1 ms (n=4) |
| -70 mV | 1.7±0.4 ms (n=5) | 2.1±0.6 ms (n=5) | 2.3±0.9 ms (n=5) | 1.1±0.3 ms (n=4) |
| -80 mV | 2.6±0.8 ms (n=3) | 4.7±1.0 ms (n=4) | 2.0±0.1 ms (n=3) | 1.5±0.5 ms (n=3) |

B

| Slow Tau | | | | |
|---|---|---|---|---|
| Command Voltage ($V_C$) | Control | 10 nM ATX II | 1 mM $H_2O_2$ | 100 μM $H_2O_2$ |
| -60 mV | 18.5±2.8 ms (n=5) | 16.7±2.3 ms (n=5) | 18.3±1.5 ms (n=5) | 20.2±5.7 ms (n=4) |
| -70 mV | 16.0±4.0 ms (n=5) | 20.3±5.3 ms (n=5) | 12.6±3.8 ms (n=5) | 19.7±4.4 ms (n=4) |
| -80 mV | 20.2±6.4 ms (n=3) | 21.4±5.6 ms (n=4) | 12.0±3.7 ms (n=3) | 18.8±6.5 ms (n=3) |

**Table 3: Effects on Inactivation in HEK293 cells.** Effects of 10 nM ATX II, 1 mM $H_2O_2$, and 100 μM $H_2O_2$ on fast inactivation tau (A) and slow inactivation tau (B) relative to control transfected HEK293 cells. Values represent the mean ± standard error mean.

and normalized area under the curve. In regards to $H_2O_2$, an opposite effect was observed with both concentrations; whereby a non-significant decrease in slow tau occurred as voltage steps became smaller (Figure 7B, D, F; Table 3B). It is likely that this decrease in slow tau inactivation in lower voltages accounts for the voltage-independent effect of $H_2O_2$ on normalized area under the curve, and presents a possible fundamental difference in the cellular targets of ATX II compared to $H_2O_2$.

## Cardiac Myocytes and Transfected HEK293 Cells Current-Voltage Relationship

After examining an inward $Na^+$ current in transfected HEK293 cells, I wanted to examine VGSC current in cardiac myocytes using the same methods and test any possible differences between the cell types. Using protocols with an identical holding potential (-160 mV), and near-identical command voltages, I was able to compare and contrast the biophysical properties between transfected HEK293 cells and cardiac myocytes.

However, given the abundance of unique ion channels in a cardiac myocyte, it was imperative to confirm that the resulting inward current was from VGSCs. Therefore, 1.5 μM TTX was applied to a single cell in order to determine if the current could be attenuated. I noticed a substantial decrease in the amount of inward current in the recording after 5 minutes (Figure 8a). Quantitatively, this was determined to be a 59.5% reduction in total current when compared to time=0 (Figure 8B).

When comparing the current-voltage relationships of transfected HEK293 cells and cardiac myocytes, I saw that cardiac myocytes were shifted +10 mV compared to transfected HEK293 cells (Figure 9A). This 10 mV required that I create a new command voltage (-50mV) for cardiac myocytes, such that peak current could be calculated and compared to transfected HEK293 cells. More specifically, for transfected HEK293 cells (n=5), the command voltages

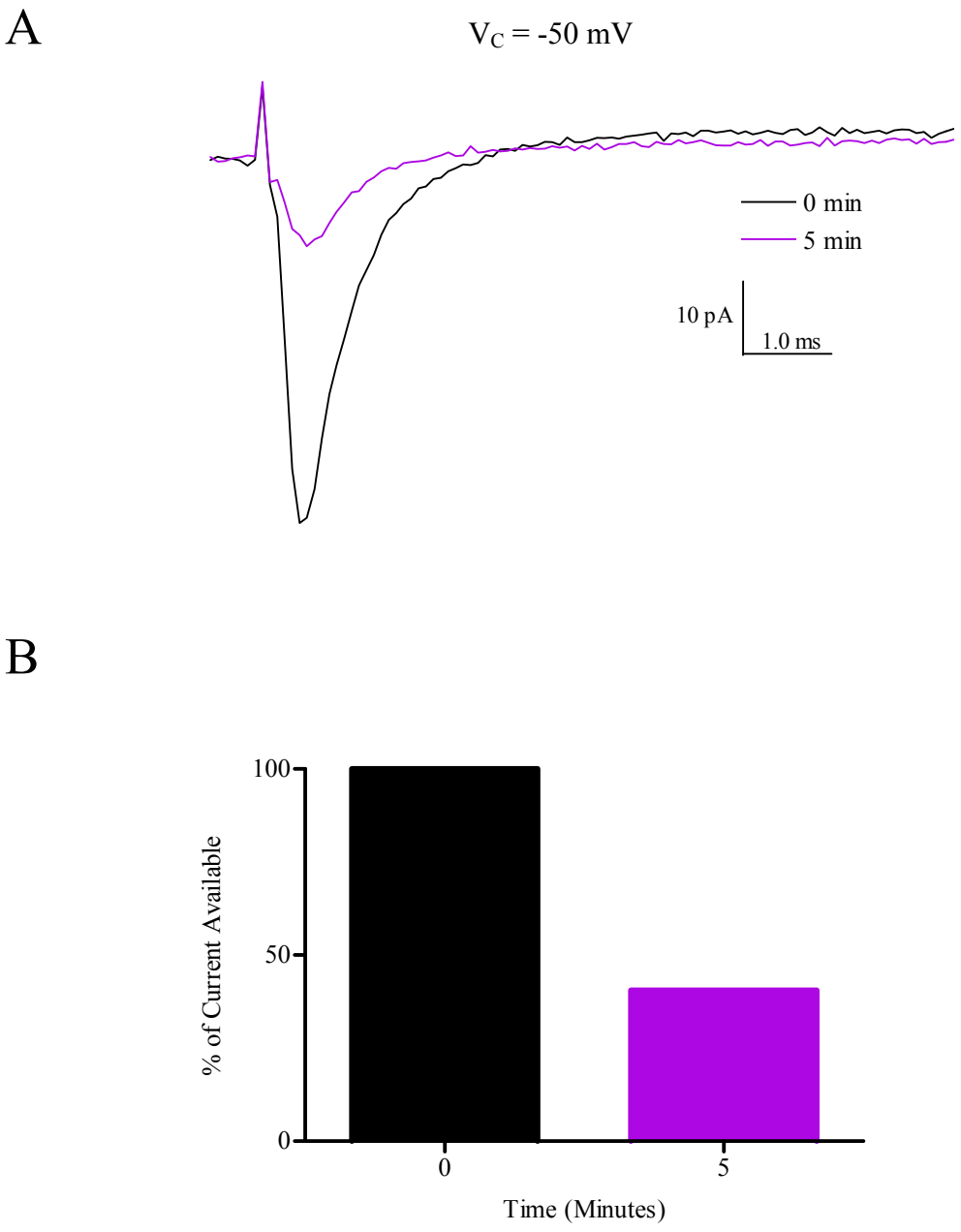


**Figure 8: Effects of 1.5 µM TTX on Cardiac Myocyte Current.** (A): Representative data illustrating the large reduction in cardiac myocyte current after 5 minutes of 1.5 µM TTX exposure. Note: the protocol that elicited this response had a voltage step of -160 mV to -50 mV; which was the largest step of the IV protocols. (B): Effect of 1.5 µM TTX on total available current after 5 minutes of exposure using the same protocol listed in A.

A

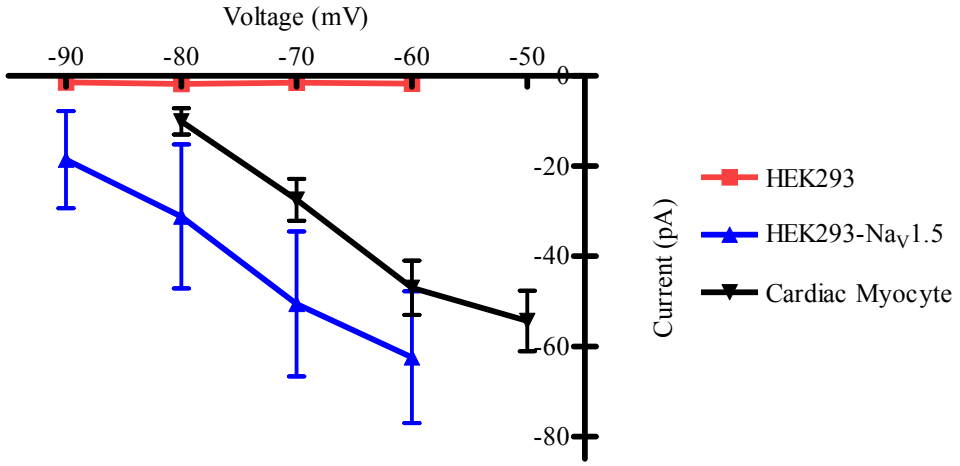


B

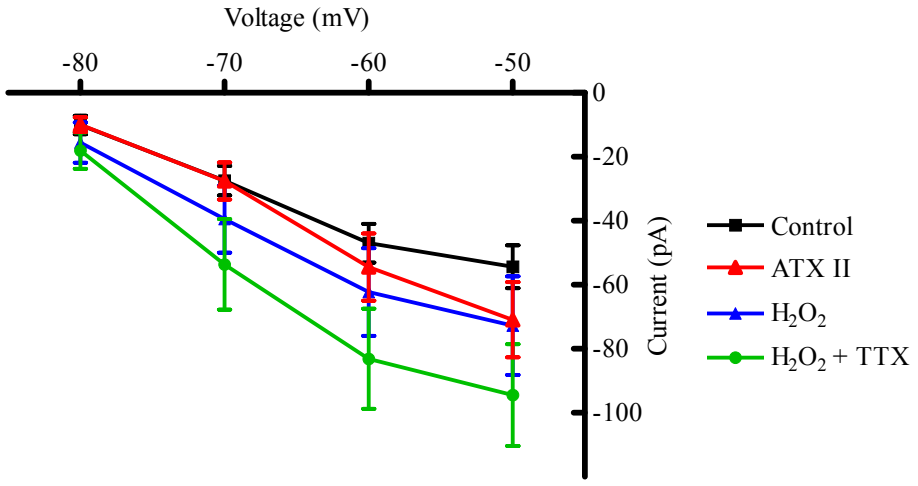


**Figure 9: Current-Voltage (IV) Relationships in Cardiac Myocytes.** (A): Comparison of IV relationships for peak $I_{Na}$ between non-transfected HEK293 cells (n=5) and transfected HEK293 cells (n=5) and cardiac myocytes (n=10). Note the voltage shift between transfected HEK293 cells and cardiac myocytes. (B): Effects of 10 nM ATX II (n=5; red), 200 µM $H_2O_2$ (n=10; blue) and 200 µM $H_2O_2$ with 10 nM TTX (n=6; green) on peak $I_{Na}$ relative to control (n=10; black) in cardiac myocytes. Values represent the mean ± standard error mean.

($V_C$) of -60 mV, -70 mV, -80 mV and -90 mV resulted in inward currents of -62.4±14.6 pA, -50.6±16.1 pA, -31.2±16.0 pA, and -18.6±10.8 pA, respectively. For cardiac myocytes (n=10), the command voltages ($V_C$) of -50 mV, -60 mV, -70 mV and -80 mV resulted in inward currents of -54.4±6.7 pA -47.0±6.0 pA, -27.5±4.6 pA, and -10.1±2.9 pA, respectively.

### Effects of ATX II, $H_2O_2$ and $H_2O_2$ with low dose TTX on Cardiac Myocytes

After identifying a voltage shift in the IV curves between transfected HEK293 cells and cardiac myocytes, I wanted to identify any possible IV shifts that might occur in cardiac myocytes under the influence of ATX II, $H_2O_2$ or $H_2O_2$ with TTX. I once again used 10 nM ATX II in order to induce $I_{Na(P)}$ in myocytes in an identical fashion to the $I_{Na(P)}$ seen in transfected HEK293 cells. In regards to $H_2O_2$, the highest dose without a lethal response was 200 μM. This was therefore the concentration used through all the experiments. I anticipated that this concentration would induce a $I_{Na(P)}$ in myocytes, as it has done in many other studies, and therefore also paired it with 10 nM TTX in a separate trial. This TTX concentration was shown in previous studies (Ward & Giles, 1997), as well as previously in our own lab, to cease the $H_2O_2$-induced $I_{Na(P)}$.

### Effects of ATX II, $H_2O_2$ and $H_2O_2$ + TTX on the Current-Voltage Relationship in Cardiac Myocytes

I initially examined any effects that 10 nM ATX II (n=5), 200 μM $H_2O_2$ (n=10), and 200 μM $H_2O_2$ + 10 nM TTX (n=6) might exert on the control (n=10) current-voltage (IV) relationship (Figure 9B; Table 4). Beginning with control cardiac myocytes, command voltages ($V_C$) of -50 mV, -60 mV, -70 mV and -80 mV resulted in inward currents of -54.4±6.7 pA, -47.0±6.0 pA, -27.5±4.6 pA, and -10.1±2.9 pA, respectively. These currents followed the same voltage-dependence observed in the current-voltage relationship of transfected HEK293 cells, and once

| Command Voltage ($V_C$) | Control | 10 nM ATX II | 200 μM $H_2O_2$ | 200 μM $H_2O_2$ + 10 nM TTX |
|---|---|---|---|---|
| -50 mV | -54.4±6.7 pA | -70.9±11.7 pA | -72.7±15.4 pA | -94.5±15.9 pA |
| -60 mV | -47.0±6.0 pA | -54.5±10.5 pA | -62.2±13.7 pA | -83.1±15.7 pA |
| -70 mV | -27.5±4.6 pA | -27.5±5.8 pA | -39.5±10.4 pA | -53.6±14.2 pA |
| -80 mV | -10.1±2.9 pA | -9.9±2.3 pA | -15.6±6.3 pA | -18.1±5.7 pA |

**Table 4: Current-Voltage (IV) Relationship in Cardiac Myocytes**. Effects of 10 nM ATX II (n=5), 200 μM $H_2O_2$ (n=10) and 200 μM $H_2O_2$ with 10 nM TTX (n=6) on peak $I_{Na}$ relative to control (n=10) in cardiac myocytes. Values represent the mean ± standard error mean.

again this effect was conserved with all experimental groups. When examining the effects of 10 nM ATX II, I saw a non-significant increase in peak values across the two largest command voltages and no difference observed between the two smallest command voltages. With regards to 200 μM $H_2O_2$, and 200 μM $H_2O_2$ + 10 nM TTX, I saw a non-significant increase in peak amplitude across all voltages in both settings.

**Effects of ATX II, $H_2O_2$ and $H_2O_2$ + TTX on Normalized Area under the Curve in Cardiac Myocytes**

As anticipated from the results of transfected HEK293 cells, the IV curves for 10 nM ATX II, 200 μM $H_2O_2$, and 200 μM $H_2O_2$ with 10 nM TTX were not significantly different from the IV curve for control cardiac myocytes. However, I once again found that there were discrepancies amongst peak current values for all compounds and myocytes. Therefore, in order to account for varying peak current and maintain the same method of analysis completed in transfected HEK293 cells, I normalized peak current to area under the curve and compared the resulting relative AUC between treatment trials and control settings.

When examining the effects of 10 nM ATX II (n=5), 200 μM $H_2O_2$ (n=10), and 200 μM $H_2O_2$ with 10 nM TTX (n=6) on control (n=10) normalized area under the curve, I saw some striking differences (Figure 10, Figure 11; Table 5). Starting with control ventricular myocytes, command voltages ($V_C$) of -50 mV, -60 mV, -70 mV and -80 mV resulted in normalized area under the curve values of -1.4±0.2 relative AUC, -2.4±0.3 relative AUC, -4.8±0.7 relative AUC, and -9.2±1.5 relative AUC, respectively. These values indicate that area under the curve exhibits voltage-dependence and this effect was preserved in all experimental groups. However, contrasting the current-voltage (IV) relationship data, a smaller voltage step elicited more normalized area under the curve. This was an identical trend to what was observed in transfected

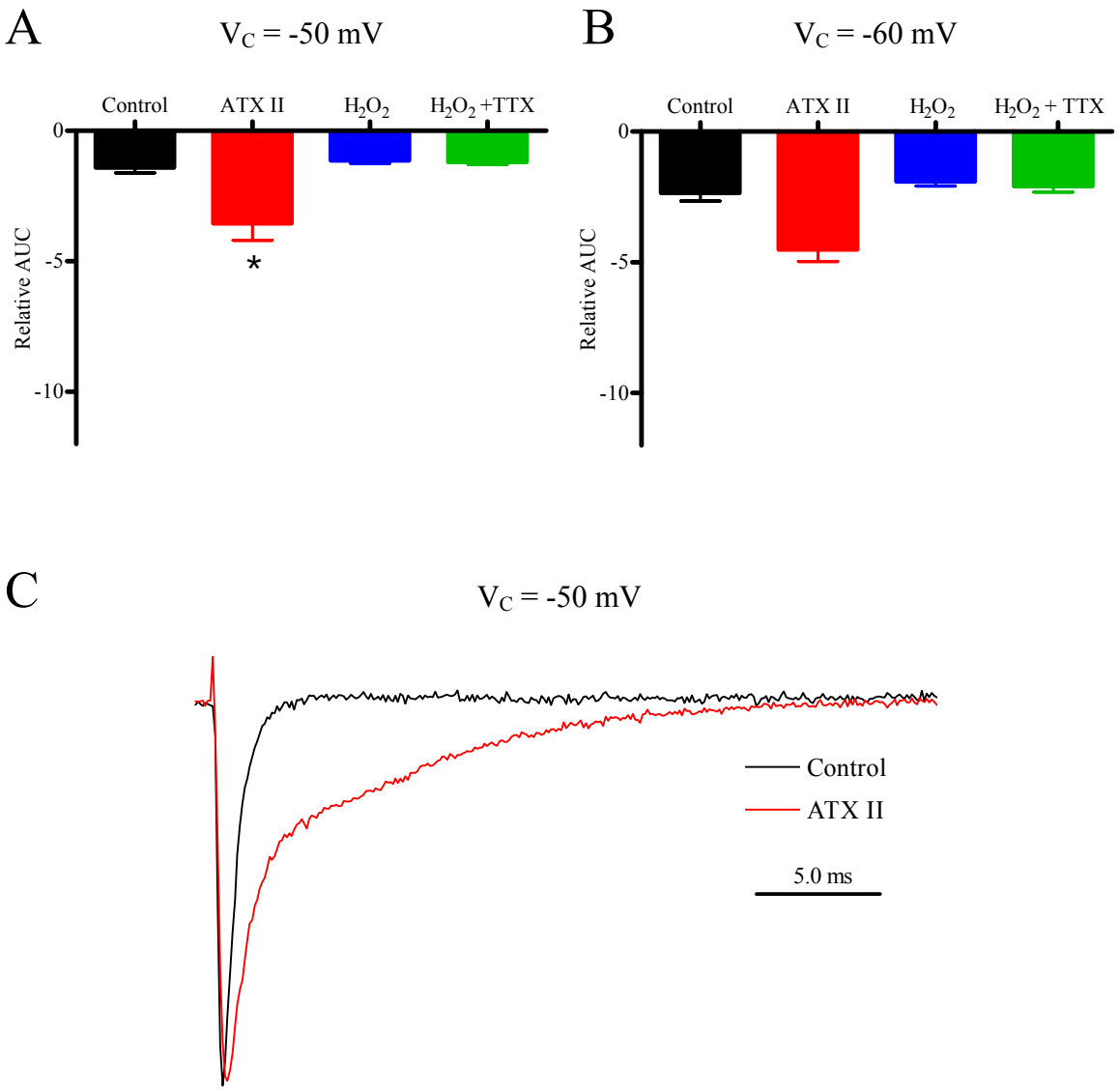


**Figure 10: Cardiac Myocyte Normalized Area under the Curve (AUC) i.** (A): Effects of 10 nM ATX II (n=5; red), 200 µM $H_2O_2$ (n=10; blue) and 200 µM $H_2O_2$ with 10 nM TTX (n=6; green) on normalized area under the curve relative to control (n=10; black) in cardiac myocytes at the command voltage ($V_C$) -50 mV. (B): Effects of 10 nM ATX II (n=5; red), 200 µM (n=10; blue) and 200 µM $H_2O_2$ with 10 nM TTX (n=6; green) on normalized area under the curve relative to control (n=10; black) in cardiac myocytes at $V_C$ -60 mV. (C): Representative data illustrating the significant effect of 10nM ATX II on area under the curve in cardiac myocytes at $V_C$ -50 mV. Note that peak amplitude in this sample trace has been normalized to 1.0 for both ATX II and control cardiac myocytes. Values represent the mean ± standard error mean. * indicates data significantly from control data ($P<0.05$).

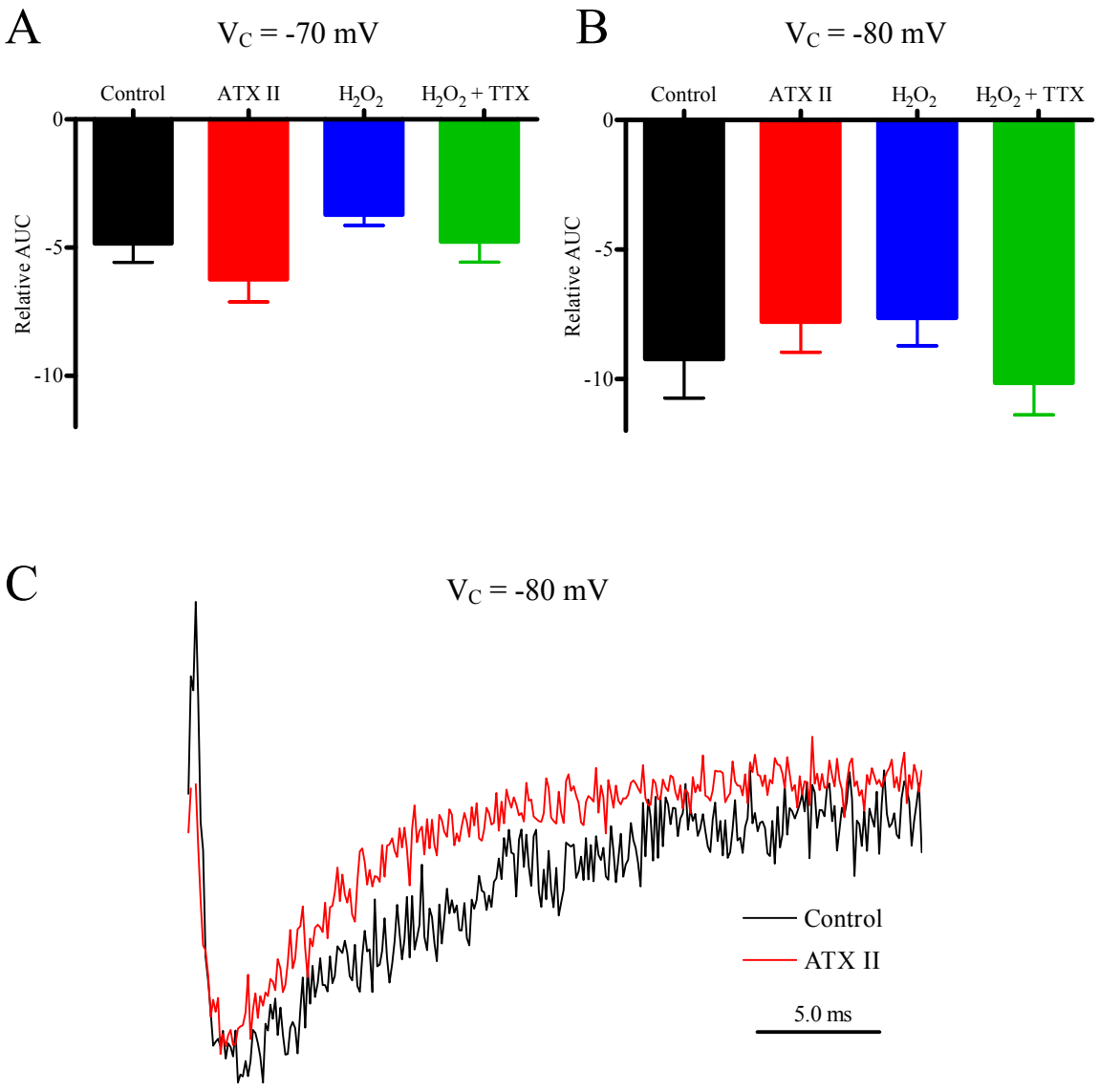


**Figure 11: Cardiac Myocyte Normalized Area under the Curve (AUC) ii.** (A): Effects of 10 nM ATX II (n=5; red), 200 µM $H_2O_2$ (n=10; blue) and 200 µM $H_2O_2$ with 10 nM TTX (n=6; green) on normalized area under the curve relative to control (n=10; black) in cardiac myocytes at the command voltage ($V_C$) -70 mV. (B): Effects of 10 nM ATX II (n=5; red), 200 µM (n=10; blue) and 200 µM $H_2O_2$ with 10 nM TTX (n=6; green) on normalized area under the curve relative to control (n=10; black) in cardiac myocytes at $V_C$ -80 mV. (C): Representative data illustrating the lack of effect of ATX on cardiac myocyte sodium current at $V_C$ -80 mV; indicating that ATX II is a voltage-dependent agent. Note that peak amplitude in this sample trace has been normalized to 1.0 for both ATX II and control cardiac myocytes. Values represent the mean ± standard error mean.

| Command Voltage ($V_C$) | Control | 10 nM ATX II | 200 μM $H_2O_2$ | 200 μM $H_2O_2$ + 10 nM TTX |
|---|---|---|---|---|
| -50 mV | -1.4±0.2 | -3.5±0.7* | -1.1±0.1 | -1.2±0.1 |
| -60 mV | -2.4±0.3 | -4.5±0.5 | -1.9±0.2 | -2.1±0.2 |
| -70 mV | -4.8±0.7 | -6.2±0.9 | -3.7±0.4 | -4.8±0.8 |
| -80 mV | -9.2±1.5 | -7.8±1.2 | -7.6±1.1 | -10.2±1.2 |

**Table 5: Normalized Area under the Curve (AUC) in Cardiac Myocytes.** Effects of 10 nM ATX II (n=5), 200 μM $H_2O_2$ (n=10) and 200 μM $H_2O_2$ + 10 nM TTX (n=5) on normalized area under the curve relative to control (n=10) cardiac myocytes. Values represent the mean ± standard error mean. * indicates data significantly different from control data ($P<0.05$).

HEK293 cells. Differences in normalized area under the curve between the cell types arose in their treatment responses. In regards to ATX II, peak command voltage ($V_C$ -50 mV) normalized area under the curve (-3.5±0.7 relative AUC) was significantly different to that of control (-1.4±0.2 relative AUC) (Figure 10A; Table 5). This effect is highlighted in the sample trace given in Figure 10C. However, testing ATX-II through the remaining three command voltages shows that the effect of ATX-II is weakened as voltage steps become less severe, with no effect being observed at the lowest command voltage (Figure 10B, Figure 11A, B; Table 5). This loss of effect at the lowest command voltage is highlighted in the sample trace shown in Figure 11C. When analyzing the potential effects of 200 μM $H_2O_2$ and 200 μM $H_2O_2$ with 10 nM TTX, I saw no effect in either the voltage-dependence or amount of relative area under the curve when compared to control settings. Both of these compounds, therefore, have had no visible effect on ventricular myocytes.

**Effects of ATX II, $H_2O_2$ and $H_2O_2$ + TTX on the Time-Dependence of Inactivation in Myocytes**

After observing a significant effect between ATX II and control myocytes for normalized area under the curve at peak command voltage ($V_C$ -50 mV), and a loss of the effect at the lowest command voltage ($V_C$ -90 mV), I wanted to characterize the tau values to see if the inactivation time constants would support this result. As was the case for transfected HEK293 cells, I could only test inactivation tau for the three largest command voltages ($V_C$ -50 mV, -60 mV and -70 mV). At $V_C$ -80 mV, the current was too small the decay was contaminated by noisew. Once again, the current decay fit a binomial exponential curve, which produced fast and slow time constants.

Beginning with fast tau, the time constants under control settings at $V_C$ -50 mV, -60 mV and -70 mV were 0.8±0.1 ms, 1.4±0.2 ms, and 3.4±0.7 ms, respectively (Figure 12A, C, E; Table 6A). These data depict an identical voltage-dependence to that observed in normalized area under the curve. In regards to the experimental groups, the data for fast tau inactivation produces near identical results to those seen in normalized area under the curve. I saw the same voltage-dependence in all groups, however, the significant effect observed in 10 nM ATX-II was lost at all voltages (Figure 12A, C, E; Table 6A). Therefore, it appears that fast tau decay in myocytes greatly influences normalized area under the curve, an effect that was also observed in transfected HEK293 cells.

Regarding slow tau, the time constants under control parameters at command voltages ($V_C$) -50 mV, -60 mV, and -70 mV were 8.2±1.5 ms, 9.4±1.1 ms, and 8.5±1.8 ms, respectively (Figure 12B, D, F; Table 6B). As can be seen from this data, there is no voltage-dependence, and thus, slow tau appears to be constant throughout an IV curve. This trend was conserved throughout the experimental groups, as no change in voltage gave a pronounced change in the time constant. (Figure 7B, D, F; Table 3B). Thus, in myocytes, slow tau inactivation remains unaltered between control and treatment settings, and cannot account for the significant effect observed in area under the curve analysis.

## Transfected HEK293 Cells vs. Cardiac Myocyte Inactivation

At this juncture, I have identified a shift in the IV curves between transfected HEK293 cells and cardiac myocytes, as well as differences in their responses to 10 nM ATX-II. Therefore, in order to completely examine any differences between these cells, I wanted to directly compare the fast and slow time constants of inactivation under control settings. If any such differences arise, I would expect them to carry over into normalized area under the curve analysis. Given

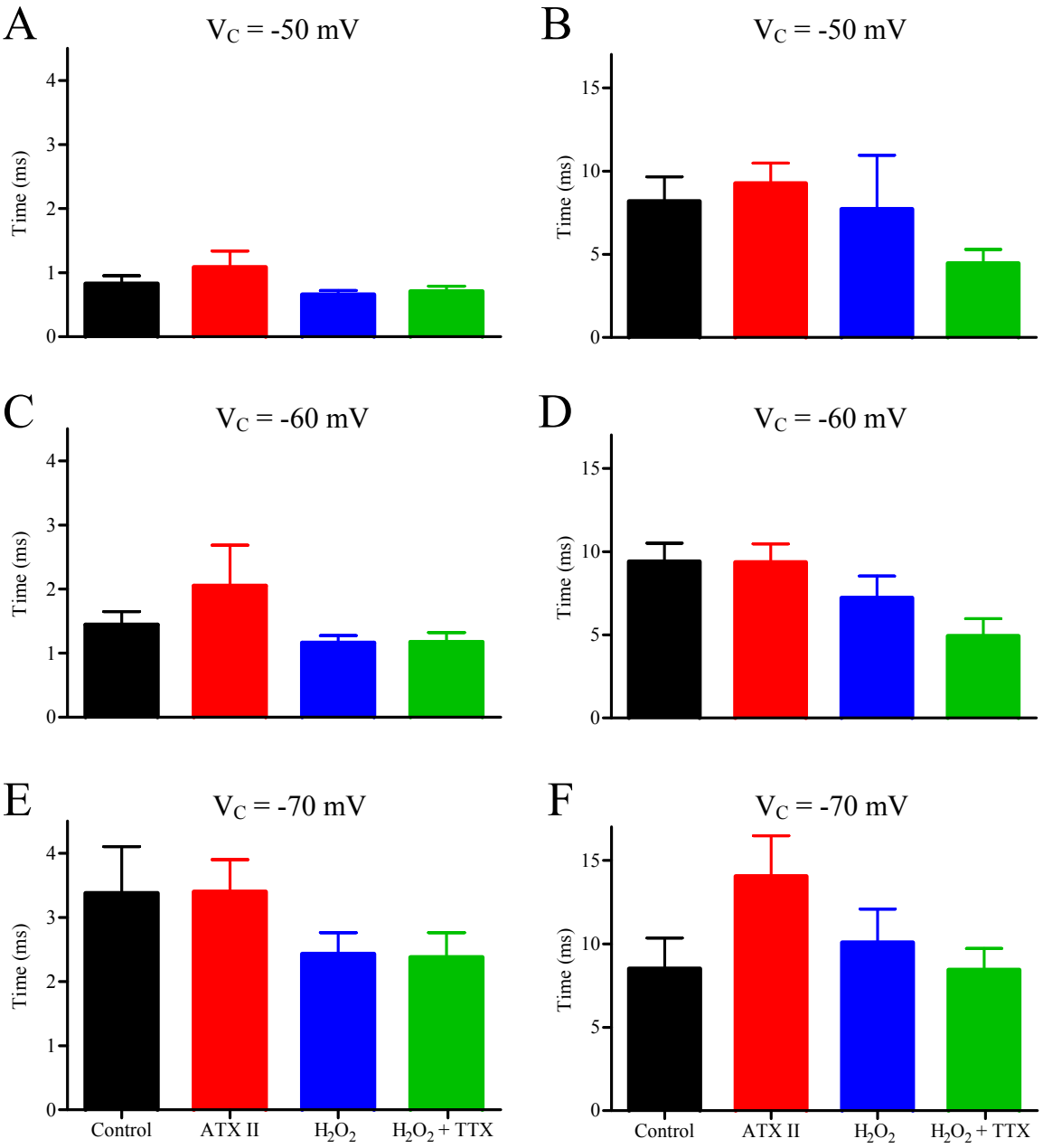


**Figure 12: Effects on Inactivation in Cardiac Myocytes.** Effects of 10nM ATX II (red), 200 µM $H_2O_2$ (blue) and 200 µM $H_2O_2$ with 10 nM TTX (green) on fast tau decay (inactivation) relative to control (n=10; black) in cardiac myocytes at the command voltage ($V_C$) -60 mV (A), $V_C$ -70 mV (C) and $V_C$ -80 mV (E). Effects of 10 nM ATX II (red), 200 µM $H_2O_2$ (blue) and 200 µM $H_2O_2$ with 10 nM TTX (green) on slow tau decay (inactivation) relative to control (black) in cardiac myocytes at the command voltage ($V_C$) -60 mV (B), $V_C$ -70 mV (D), and $V_C$ -80 mV (F). Values represent the mean ± standard error mean.

A

| Fast Tau | | | | |
|---|---|---|---|---|
| Command Voltage ($V_C$) | Control | 10 nM ATX II | 200 μM $H_2O_2$ | 200 μM $H_2O_2$ + 10 nM TTX |
| -50 mV | 0.8±0.1 ms (n=10) | 1.1±0.2 ms (n=5) | 0.7±0.1 ms (n=10) | 0.7±0.1 ms (n=5) |
| -60 mV | 1.4±0.2 ms (n=10) | 2.1±0.6 ms (n=5) | 1.2±0.1 ms (n=10) | 1.2±0.2 ms (n=5) |
| -70 mV | 3.4±0.7 ms (n=8) | 3.4±0.5 ms (n=4) | 2.4±0.3 ms (n=10) | 2.4±0.4 ms (n=5) |

B

| Slow Tau | | | | |
|---|---|---|---|---|
| Command Voltage ($V_C$) | Control | 10 nM ATX II | 200 μM $H_2O_2$ | 200 μM $H_2O_2$ + 10 nM TTX |
| -50 mV | 8.2±1.5 ms (n=10) | 9.3±1.2 ms (n=5) | 7.7±3.2 ms (n=10) | 4.5±0.8 ms (n=5) |
| -60 mV | 9.4±1.1 ms (n=10) | 9.4±1.1 ms (n=5) | 7.2±1.3 ms (n=10) | 4.9±1.1 ms (n=5) |
| -70 mV | 8.5±1.8 ms (n=6) | 14.0±2.4 ms (n=4) | 10.1±2.0 ms (n=9) | 8.4±1.3 ms (n=5) |

**Table 6: Effects on Inactivation in Cardiac Myocytes.** Effects of 10 nM ATX II, 200 μM $H_2O_2$, and 200 μM $H_2O_2$ + 10 nM TTX on fast inactivation tau (A) and slow inactivation tau (B), relative to control cardiac myocytes. Values represent the mean ± standard error mean.

that there is a shift in the IV curves, I examined tau decay values at peak current ($V_C$ -50 mV for cardiac myocytes; $V_C$ -60 mV for transfected HEK293 cells).

Starting with fast tau, at voltages that elicited peak current, the time constant for transfected HEK293 cells (n=5) was 1.3±0.2 ms. The time constant for cardiac myocytes (n=10) was 0.8±0.1 ms. These values fell just short of significance.

When examining slow tau at the same voltages, the time constant for transfected HEK293 cells (n=5) was 18.5±2.8 ms; while the time constant for cardiac myocytes (n=10) was 8.2±1.5 ms (Figure 13A). These values were significantly different to one another, indicating that $I_{Na}$ in transfected HEK293 cells inactivates at a slower rate compared to ventricular cardiac myocytes. A sample trace identifying the different inactivation profiles is given in Figure 13C.

Given that $I_{Na}$ in transfected HEK293 cells inactivates at a slower rate compared to cardiac myocytes, I would expect the current in transfected HEK293 cells would have a larger relative AUC than a cardiac myocyte in the normalized area under the curve analysis. By comparing the normalized values at peak current, I observed a significant difference between transfected HEK293 cells and cardiac myocytes. The precise values were: transfected HEK293 cells (n=5): -3.6±0.8 relative AUC and cardiac myocytes (n=10): -1.4±0.8 relative AUC (Figure 13B).

## Voltage-Dependence of Inactivation

After identifying different time constants of inactivation between transfected HEK293 cells and cardiac myocytes, I wanted to directly examine the voltage-dependence of inactivation in both cell types. In order to achieve this, I used different protocols that are designed to inactivate channels first, and then test how many can open using a test pulse. For both

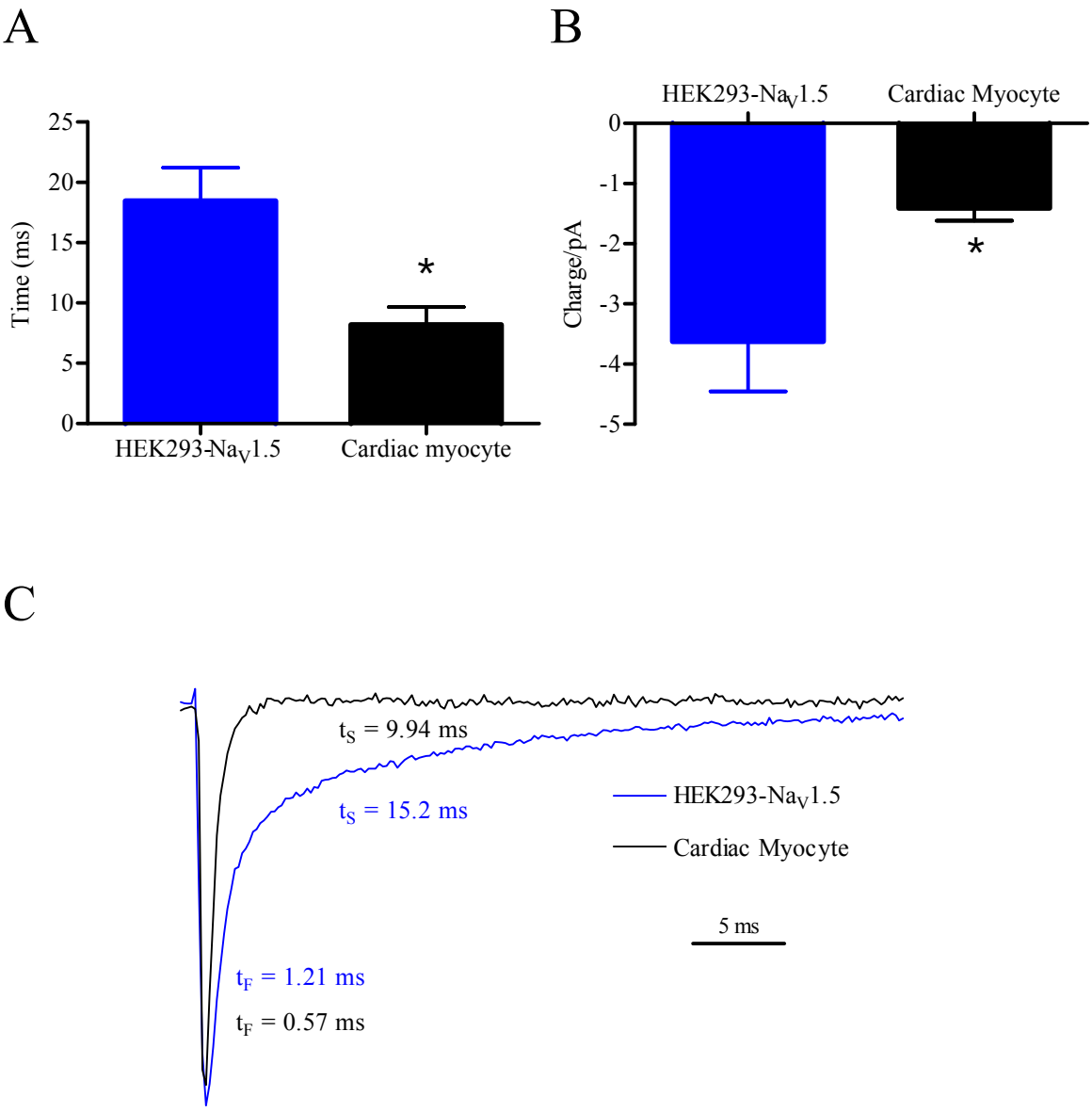


**Figure 13: Transfected HEK293 cells vs. Cardiac Myocyte Inactivation.** (A): Comparison of the slow tau decay between transfected HEK293 cells (n=5) and cardiac myocytes (n=10) at the largest voltage step for each cell type. (B): Comparison of the normalized area under the curve between transfected HEK293 cells (n=5) and cardiac myocytes (n=10) at the largest voltage step for each cell type. (C): Representative data illustrating the different inactivation taus (and thus differing inactivation profile) between transfected HEK293 cells and cardiac myocytes at the largest voltage step. Values represent the mean ± standard error mean. * indicates data significantly from control data ($P<0.05$).

cells types, I used holding potentials ($V_H$) of -160 mV, -140 mV and -120 mV, followed by a step to a much more positive potential.

## Voltage-Dependence of Inactivation in HEK293 cells

The first experiments successfully proved that non-transfected HEK293 cells have no current and, therefore, have no voltage-dependence of inactivation. The amount of current recorded was insignificant from 0 pA ($P>0.05$; $n=5$). A sample trace is provided in Figure 14A. When examining transfected HEK293 cells, a large current is observed at $V_H$ -160 mV, followed by a smaller current at $V_H$ -140 mV, and finally, little to no current at $V_H$ -120 mV (Figure 14B). These values were significantly different from 0 pA ($P<0.05$, $n=5$) and form a traditional steady-state model of inactivation (Figure 14C).

## Effects of ATX II and $H_2O_2$ on the Voltage-Dependence of Inactivation in Transfected HEK293 cells

After successfully proving that the protocols described above produce a steady-state inactivation curve, and that non-transfected HEK293 cells have no current, I tested if the same treatments described earlier would affect the voltage-dependence of inactivation in transfected HEK293 cells. As can be seen from Figure 14C, there is no shift in any of the inactivation curves, indicating that none of the experimental trials had any effect on the voltage-dependence of inactivation.

## Voltage-Dependence of Inactivation in Transfected HEK293 Cells and Cardiac Myocytes

Given the differences in normalized area under the curve and inactivation tau already highlighted, I directly compared the voltage-dependence of inactivation between transfected

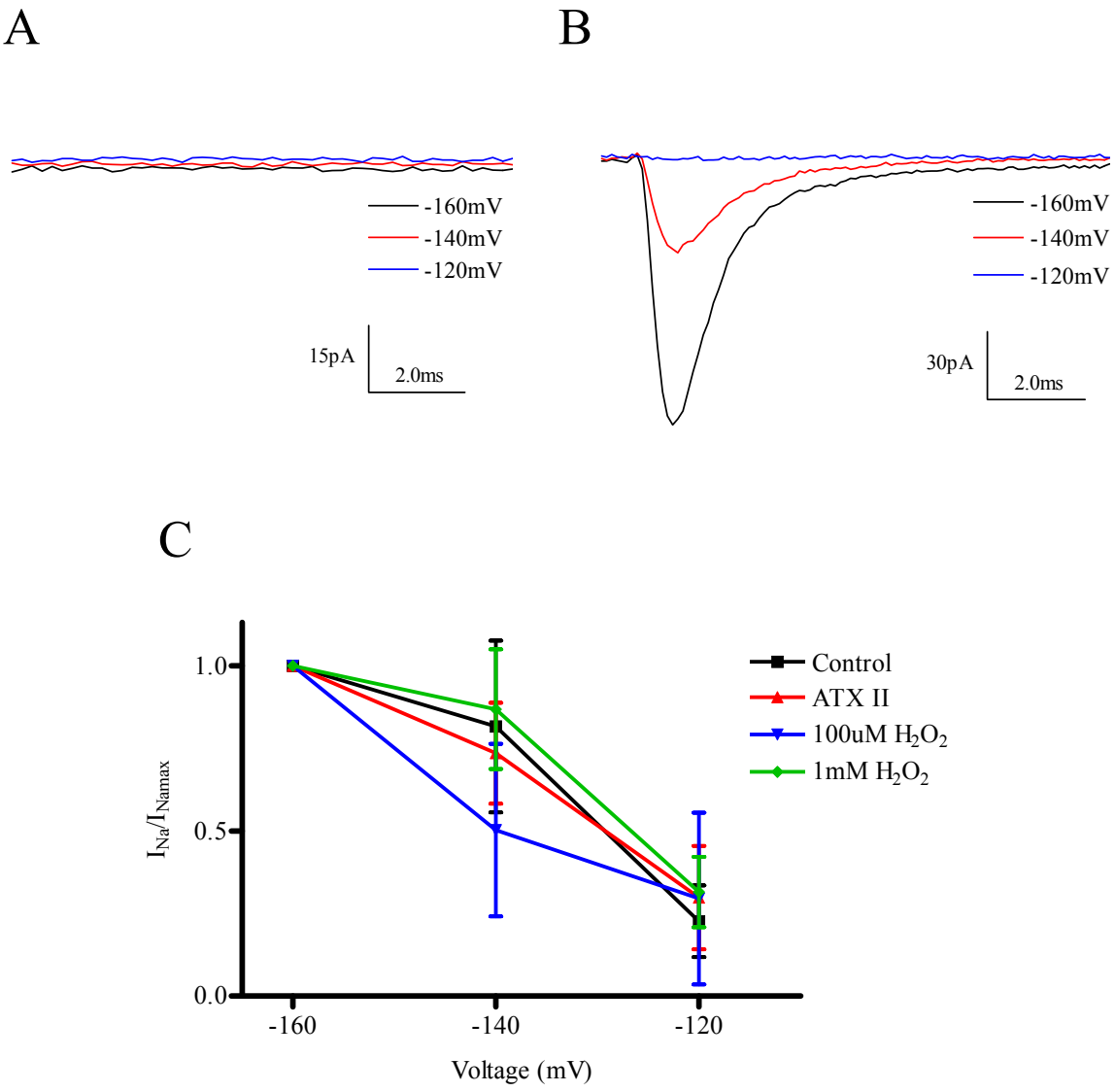


**Figure 14: Voltage-Dependence of Inactivation in HEK293 cells**. (A): Representative data illustrating the voltage-dependence of inactivation in non-transfected HEK293 cells. The current observed is not different from 0 ($p>0.05$; n=5). Note: this trace is cropped between 120 ms and 130 ms of the protocol, the time period where an effect was observed. (B): Representative data illustrating the voltage-dependence of inactivation in transfected HEK293 cells. Note: this trace is cropped between 120 ms and 130 ms of the protocol. (C): Effects of 10 nM ATX II (n=3; red), 100 µM $H_2O_2$ (n=3; blue) and 1 mM $H_2O_2$ (n=5; green) on the voltage-dependence of inactivation relative to control (n=5; black) in transfected HEK cells. Values represent the mean ± standard error mean.

HEK293 cells and cardiac myocytes. However, because cardiac myocytes fit a Boltzmann distribution and transfected HEK293 cells did not, I could not fit and compare the curves. Thus, all values were extrapolated from the line of best fit on the graph, and could not be statistically tested. Based the data extrapolated, I found a complete rightward shift of the inactivation curve (approximately 20 mV) of cardiac myocytes (Figure 15A). This shift required another protocol for cardiac myocytes, $V_H$ -110 mV, so that the curve could decay past 50%. The resulting $V_{50}$ values were: for transfected HEK 293 cells, approximately -130 mV and for cardiac myocytes, approximately -113 mV.

## Effects of ATX II, $H_2O_2$ and $H_2O_2$ + TTX on the Voltage-Dependence of Inactivation in Cardiac Myocytes

Once observing a dramatic difference in the voltage-dependence of inactivation between transfected HEK293 cells and cardiac myocytes, I wanted to determine if pharmacological intervention could affect the voltage-dependence of inactivation in myocytes, given that it had no effect in transfected HEK293 cells. I once again found no voltage shift in the any of the experimental trials when compared to control myocytes (Figure 15B), indicating that none of these treatments impacted the voltage-dependence of inactivation in cardiac myocytes.

A

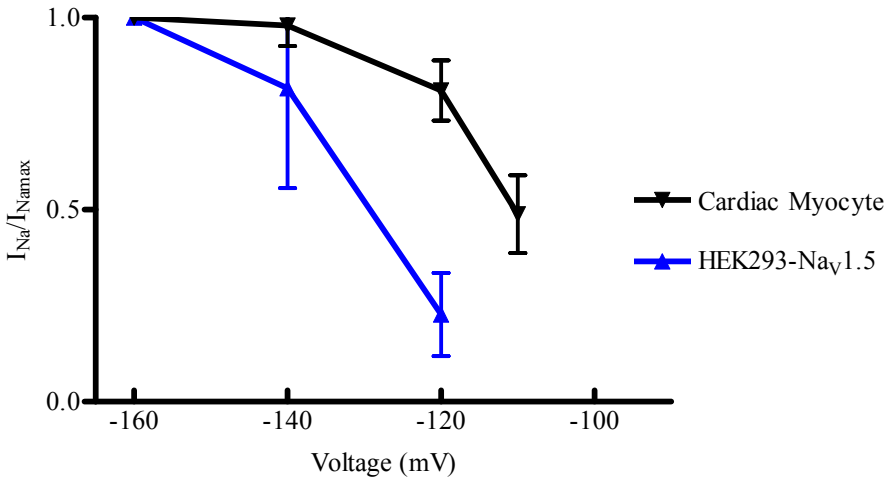


B

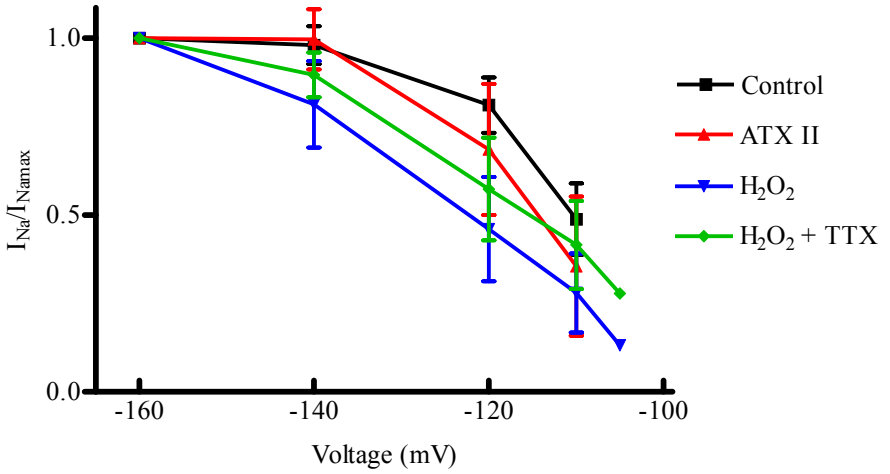


**Figure 15: Voltage-Dependence of Inactivation in Cardiac Myocytes.** (A): Comparison of the voltage-dependence of inactivation between transfected HEK293 cells (n=5) and cardiac myocytes (n=7). Note the 20 mV voltage shift between transfected HEK293 cells and cardiac myocytes. (B): Effects of 10 nM ATX II (n=3; red), 200 µM $H_2O_2$ (n=4; blue) and 200 µM $H_2O_2$ with 10 nM TTX (n=4; blue) on the voltage-dependence of inactivation relative to control (n=7; black) in cardiac myocytes. Values represent the mean ± standard error mean.

# Chapter 5

# Discussion

In the heart, $I_{Na(P)}$ has been shown associated with hypoxia (Haigney *et al.*, 1994) or ischemia reperfusion injury (Ferrari *et al.*, 2004), and likely results from an increased production of reactive oxygen species (Zweier *et al.*, 1987) during these pathologies. Of all the possible reactive oxygen species, $H_2O_2$ is believed to be the most important because of its stability and neutral charge (Ward & Giles, 1997). This, combined with the molecules small size, allows it to freely pass membranes and enter cells. How $H_2O_2$ can cause such drastic changes in VGSC function is of debate and currently unclear. Previous data in our own lab supports the theory that multiple VGSC isoforms are present in the heart, and specific isoforms can enter a persistent mode under the right environment (Reviewed in Saint, 2008). The two most prevalent isoforms in the heart are $Na_v1.5$ and $Na_v1.1$ (Reviewed in Saint, 2008), although $Na_v1.1$ only contributes approximately 5% of the total $Na^+$ current (Maier *et al.*, 2002). $Na_v1.1$, traditionally a CNS VGSC, is known to readily enter a persistent mode with burst openings and this function is normal in the CNS (Kalume *et al.*, 2007). In the heart, however, burst openings and persistent current would be deleterious as channels need to open, rapidly close and reprime for the next beat to occur. Given the unclear nature and potential lethal effects of a $I_{Na(P)}$, I sought out to explore the theory presented above by comparing transfected $Na_v1.5$ in HEK293 cells to native ventricular myocytes under control, ATX II, $H_2O_2$, and $H_2O_2$ + TTX settings.

The major challenge with researching and testing $I_{Na(P)}$ was finding an electrophysiological technique to examine the biophysical properties of VGSCs. Previous studies

demonstrated that $I_{Na(P)}$ cannot be recorded using the whole-cell voltage-clamp technique (Barrington, 1994; Ward & Giles, 1997). This is because the whole-cell technique causes a dialysis of the cytoplasm, and the most accepted theory explaining $I_{Na(P)}$ relies upon PKC, an intracellular second messenger (Ward & Moffat, 1995; Ju *et al.*, 1996). Given that whole-cell voltage-clamp is ineffective, the biophysical effect of $H_2O_2$ on VGSCs is rarely tested and lacking in the literature. I, therefore, adopted macro cell-attached voltage-clamp to measure channel currents with no dialysis of the cytoplasm. In this technique, only channels that are located within the patch are recorded, and, therefore, the amount of current can vary pending channel densities and electrode diameter.

My results indicate that there are major functional differences in the inactivation properties of transfected HEK293 cells compared to cardiac myocytes. Transfected HEK293 cells was seen to inactivate at more negative voltages and at a much slower rate compared to cardiac myocytes. My results also indicate $Na_v1.5$ current is unaffected by $H_2O_2$ at physiological concentrations. I propose, therefore, that $Na_v1.5$ is not responsible for the $I_{Na(P)}$ observed under an ROS challenge, and that other VGSC isoforms must be present for the $I_{Na(P)}$ to occur.

## Marco Cell-Attached Voltage-Clamp Protocols

I selected this method of patch clamp because of its effectiveness in recording channel currents without disruption to the interior of the cell. I was able to record peak current (thus, assess current-voltage relationships), area under the curve, inactivation decay tau and test the voltage-dependence of inactivation.

In regards to peak current, area under the curve and inactivation decay tau, protocols between whole-cell and cell-attached were not very different. In whole-cell voltage-clamp, my standard protocol used to test these biophysical properties would hold the cell at -135 mV before

stepping to more positive voltages. Rarely would current be recorded at command voltages lower than -80 mV, and current would increase in a voltage-dependent manner until peak was hit at approximately -30 mV. In my cell-attached model, myocytes were held at -160 mV, with current being recorded at command voltages as low as -80 mV and continuing to rise as command voltages became more positive.

A large discrepancy occurs during the steady-state inactivation protocols. In whole-cell voltage-clamp, conditioning pulses would start at -140 mV, with VGSCs beginning to inactivate during conditioning pulse -100 mV. In the cell-attached model, inactivation began at conditioning pulse -140 mV, and was completed by conditioning pulse -105 mV. Thus, in cell-attached voltage-clamp, VGSCs inactivated at much more negative potentials compared to whole-cell voltage clamp. This effect, however, is common amongst VGSC recordings and has been documented in rat myocytes (Bodewei *et al.*, 1982; Kunze *et al.*, 1985), mouse myocytes (Benndorf *et al.*, 1985), guinea pig myocytes (Murray *et al.*, 1990), canine myocytes (Berman *et al.*, 1989) and canine Purkinje cells (Makielski *et al.*, 1987). Murray *et al.* (1990) speculated that this leftwards shift was caused by a distortion in the membrane that induced a VGSC conformational change once the patch was formed.

## Effects of ATX II and $H_2O_2$ on Transfected HEK293 cells

My first studies sought to examine any possible differences that might occur in peak current amplitude when transfected HEK 293 cells were exposed to 10n M ATX II, 100 μM $H_2O_2$ or 1 mM $H_2O_2$. My results indicate that none of these compounds significantly increased peak amplitude or shifted the IV curves (Figure 5B). This was anticipated for ATX II, as it was documented many years ago that ATX II only marginally increases and delays peak amplitude (Narahashi *et al.*, 1969). Narahashi *et al* .(1969) believed that by slowing inactivation, ATX II

allowed peak amplitude to reach a slightly larger value. The result of 100μM $H_2O_2$ causing no shift in the IV curve was particularly interesting because it has been previously shown that channel oxidation shifts the activation curve to more negative potentials (Bhatnagar *et al.*, 1990). I, therefore, would have expected to see this leftward shift if $H_2O_2$ were to oxidize VGSCs directly and induce an $I_{Na(P)}$. As this was not observed, intracellular messengers, such as PKC (Ward & Moffat, 1995; Ju *et al.*, 1996), are likely responsible for the $I_{Na(P)}$ observed in hypoxic or reperfused myocytes.

At 1 mM $H_2O_2$, there is also no shift in the IV curve, but a large reduction in current at all voltage steps. This concentration, however, killed cardiac myocytes (by removing all current and changing the morphological structure of the cell - as observed under the microscope), and is therefore unlikely to occur without a lethal response. I believe that because $H_2O_2$ can affect so many processes in the cell, this extremely high concentration targeted multiple systems and induced cell-death in myocytes. Specifically, the highly nucleophilic $H_2O_2$ is known to cause lipid peroxidation (Rubin & Farber, 1984), protein oxidation (Fliss, 1988), altered energy metabolism (Spragg *et al.*, 1985), enzyme activation (Natarajan *et al.*, 1993; Mekhfi *et al.*, 1996) and alterations in intracellular $Ca^{2+}$ concentration (Hyslop *et al.*, 1986). Given that I identified a large reduction in peak amplitude, it is very likely that 1 mm $H_2O_2$ damaged many cellular processes responsible for ion passage through the channel, and thus caused a reduction in peak current.

Following identification of no major differences in the IV relationship between 10 nM ATX II, 100 μM $H_2O_2$, 1 mM $H_2O_2$ relative to control, I wanted to examine if there were any differences in the time course of inactivation. As stated earlier, ATX II is known to increase the action potential duration in cardiac myocytes (Ravens, 1976) by effectively slowing VGSC inactivation (Narahashi *et al.*, 1969); whereas 100 μM $H_2O_2$ is known to induce a TTX-sensitive

prolonged action potential duration, likely via a PKC mechanism (Ward & Giles, 1997). It is, therefore, possible that $H_2O_2$ targets VGSC inactivation as well, and this effect could be identified via area under the curve analysis and /or comparison of tau values.

My results indicate that both compounds had a non-significant effect in both normalized area under the curve (Figure 6) and tau measurements (Figure 7). ATX II, although non-significant, did consistently have larger area under the curve recordings for multiple voltages, and this finding was also observed in my fast tau measurements. The likely reason why this was not significant is a result of the large S.E.M. As was stated earlier, the potential caveat of macro cell-attached voltage-clamp is that the current recorded is only from channels under the patch. This means that any variation in the amount of channels under the patch would create large variations in currents and, thus, a large S.E.M. When dealing with an expression system, such as HEK293 cells, the amount of channels on the membrane varies from culture to culture, and is extremely difficult to account for. The particularly relevant result from this data analysis is no effect of 100 μM $H_2O_2$ on normalized area under the curve or the tau values. Given that there are not even trends between this compound and control values, it is highly likely that 100 μM $H_2O_2$ has no effect on these cells, and thus no effect on $Na_v1.5$.

### Effects of ATX II, $H_2O_2$ and $H_2O_2$ + TTX on Cardiac Myocytes

Once completing the analysis of transfected HEK293 cells, I wanted to test cardiac myocytes using identical parameters and near identical treatment combinations. I directly compared the effects of 10 nM ATX II, 200 μM $H_2O_2$, and 200 μM $H_2O_2$ + 10 nM TTX. I selected 200 μM $H_2O_2$ as the dose because it had been previously shown to be non-lethal as well as be in the concentration range (50 μM - 200 μM) known to cause a prolonged action potential in myocytes (Ward & Giles, 1997). Given that there are multiple VGSC isoforms in cardiac

myocytes (Haufe *et al.*, 2005), I anticipated that $H_2O_2$ would modulate current in some capacity, and thus it was paired with 10 nM TTX. This dose has been used previously in the lab to inhibit the action potential prolongation seen under an ROS challenge.

Initially, I compared the peak current amplitudes of 10 nM ATX II, 200 μM $H_2O_2$, and 200 μM $H_2O_2$ + 10 nM TTX relative to control and plotted them on an IV curve (Figure 9B). There was no significant difference between any of the treatment groups relative to control. This is consistent with the IV curves of transfected HEK293 cells (Figure 5B) and was expected given the rationale presented for the transfected HEK293 data.

After observing no difference in the IV curves between all compounds and control myocytes, I examined the effects of each treatment on the time course of inactivation, with the intent of comparing the results to what was observed in transfected HEK293 cells. The normalized area under the curve analysis showed two very different results for myocytes compared to transfected HEK293 data. First, ATX-II treated myocytes had significantly more relative AUC compared to a control myocyte at the peak voltage step (Figure 10A, C). This effect became non-significant in the next two voltage steps (Figure 10B, 11B), and was no longer present at the smallest voltage step (Figure 11A, C). These results were expected because it has been shown that ATX II binding affinity is not only voltage-dependent, but follows the same voltage-dependence of a VGSC (Catterall, 1979). Thus, as weaker voltage steps have a lower probability of opening VGSCs, the probability of ATX II binding also decreases and the effect is minimized. Secondly, I saw a much smaller S.E.M for the peak voltage steps. This adds further substance to the notion that there is large variation amongst channel densities in the expression system from culture to culture. It also shows that channel densities are rather homogenous in

cardiac myocytes as they were selected without any knowledge of their exact location in the intact heart.

The surprising result of the normalized area under the curve analysis was the 200 μM $H_2O_2$ group. Not only was there no significant difference between this treatment concentration relative to control, there was no trend at any voltage (Figure 10A, B; Figure 11A, B). I believe that $H_2O_2$ had no effect on my myocytes for two reasons: 1) $H_2O_2$ does not induce $I_{Na(P)}$ via the $Na_V1.5$ isoform (as suggested earlier), and 2) because of the low abundance of $Na_V1.1$ in myocytes. As stated in the introduction, $Na_V1.1$ accounts for only 5% of the total $Na^+$ current in a cardiac myocyte (Maier *et al.*, 2002). Given the low percentage of $Na_V1.1$ in myocytes, it is impossible to know if any of the channels under the patch are $Na_V1.1$.

## Biophysical Differences between Transfected HEK293 cells and Cardiac Myocytes

In addition to comparing the pharmacological differences between cardiac myocytes and transfected HEK293 cells, I wanted to identify any biophysical differences that might exist between the two cell groups. I found that the IV curve for transfected HEK293 cells was shifted 10 mV to the left in comparison to cardiac myocytes (Figure 9A). Also, transfected HEK293 cells had significantly more relative AUC when compared to cardiac myocytes (Figure 13B), and this effect was conserved in slow tau measurements (Figure 13A). Given that the $H_2O_2$ data could not conclusively prove that the patches had other VGSC isoforms besides $Na_V1.5$, I believe that this effect was likely a result of β subunits.

Previous studies testing $Na_V1.2$, noted that this isoform activated at more positive potentials when paired with β subunits (Qu *et al.*, 2001). Although this wasn't performed on $Na_V1.5$, it does identify that β subunits are capable of modulating VGSC activation, and could account for the shift seen in the IV curve. However, when examining the effects of β1/β3 co-

expression with $Na_V1.5$ in oocytes, it was noted that co-expressed cells shifted the IV curve 10 mV to the left compared to β subunit deprived $Na_V1.5$-oocytes (Ko *et al.*, 2005). Thus, co-expression of $Na_V1.5$-HEK293 cells with β1/β3 could shift the IV curves even further apart, should the results follow the same trends as those just presented. Given the inconsistencies in the literature, transfecting $Na_V1.5$-HEK293 cells with β1 and β3 subunits is a necessary follow-up to this study.

With regards to inactivation, previous studies testing the effects of β subunits with skeletal muscle VGSCs showed that inactivation occurred at a much slower rate in cells that were β subunit deprived (Schreibmayer *et al.*, 1994). This was also observed in β1/β3-$Na_V1.5$-oocytes, where inactivation was much quicker in coexpressed oocytes compared to β subunit deprived oocytes (Ko *et al.*, 2005). These results could explain the slower inactivation time course I observed between transfected HEK293 cells and cardiac myocytes. Given that ventricular myocytes have β1 and β3 subunits (Fahmi *et al.*, 2001), they are predicted to inactivate faster than transfected HEK293 cells lacking β subunits.

## Voltage-Dependence of Inactivation

Having observed different responses to treatments in transfected HEK293 cells and cardiac myocytes, as well as differences between the two cell types themselves, I wanted to characterize any differences that might occur in the voltage-dependence of inactivation. In order to do so, I compared the effects of different treatments to transfected HEK293 cells (Figure 14B), then treatments to cardiac myocytes (Figure 15B), and finally, transfected HEK293 cells to cardiac myocytes (Figure 15A).

When comparing the effects of 10 nM ATX II, 100 μM $H_2O_2$, 1 mM $H_2O_2$ relative to control transfected HEK293 cells, I saw no shifts in the voltage-dependence of inactivation in any

treatment relative to control (Figure 14B). These results were not surprising, as none of these compounds caused a significant effect in previous experiments. Comparing the effects of 10 nM ATX II, 200 μM $H_2O_2$, and 200 μM $H_2O_2$ + 10nM TTX relative to control myocytes showed the same results as those described in the transfected HEK293 cells (Figure 15B). This was somewhat surprising, as it is known that ATX II does reduce the steepness of the steady state inactivation curve and push it to more positive potentials (Catterall, 1979). I believe that this effect is a likely result of the different methods: Catterall (1979) performed his experiments under whole-cell voltage-clamp. Given the discrepencies presented earlier between whole-cell voltage-clamp and macro cell-attached voltage-clamp, I believe that a necessary follow up to this study would be to compare and contrast myocyte responses to ATX II under both voltage-clamp techniques. This should help to identify why ATX II had no effect on myocyte voltage-dependence of inactivation under macro cell-attached voltage-clamp.

Finally, when comparing the steady state inactivation profiles of transfected HEK293 cells to cardiac myocytes, I saw that transfected HEK293 cells shifted the curve left compared to myocytes (Figure 15A). I believe that this result is again a manifestation of no β subunits. Once again, however, the literature is inconsistent. In regards to $Na_V1.2$, it was noted that this isoform inactivated at more positive potentials when paired with β subunits (Qu *et al.*, 2001). Should this result be consistent with any data, the effect of β subunits could push the two steady-state inactivation curves together. However, when examining the effects of β1/β3 co-expression with $Na_V1.5$ in oocytes, it was noted that co-expressed cells shifted the steady-state inactivation curve to more negative potentials when compared to β subunit deprived $Na_V1.5$-oocytes (Ko *et al.*, 2005). Should future data follow this trend, it would push the two curves further apart.

## Future Directions

As discussed, a necessary follow up experiment is to examine the effects of transfected HEK293 cells with β1 and β3 subunits. Although a previous study did examine the effects of β1 and β3 subunits on $Na_V1.5$, it was in a non-mammalian system. Thus, it would be a large stretch to assume that mammalian cells would respond in the same manner. Also, given the inconsistent nature of the literature in regards to β subunits and their effects on activation/inactivation kinetics, this experiment could help to provide some clarity on how β subunits effect activation/inactivation, and to which way they shift the curve in $Na_V1.5$.

The most necessary future experiment would be to directly compare the effects of transfected $Na_V1.5$ in HEK293 cells to transfected $Na_V1.1$ in HEK293 cells. This is because although macro cell-attached voltage-clamp is the appropriate technique to search for $I_{Na(P)}$, I could not conclusively prove if there were any $Na_V1.1$ in my patches. The low abundance of $Na_V1.1$ made it difficult to record in the $Na_V1.5$ dominant cardiac myocytes. Thus, direct isolation of the $Na_V1.1$ current into HEK293 cells would be the best method to compare and contrast $Na_V1.1$ and $Na_V1.5$.

In theory, the best approach to isolate $Na_V1.1$ and compare its effects to control myocytes would be to culture myocytes and knock down $Na_V1.5$ using siRNA. This approach has been attempted before in the lab and failed for numerous reasons, the primary one being that myocytes are extremely difficult to culture. After only days in culture, adult myocytes begin to de-differentiate into a neonatal phenotype, which alters the complements of currents expressed at the membrane surface. Secondly, siRNA may not eliminate all of the $Na_V1.5$ channels and, thus, the resulting current from these cultured myocytes would again contain a blend of $Na_V1.1$ and some

$Na_V1.5$ currents. It is for these reasons that I believe the best method to compare and contrast $Na_V1.1$ and $Na_V1.5$ currents is through transfected HEK293 cells, with appropriate β subunits.

## Conclusion

My study examined the effects of ATX II, $H_2O_2$ and $H_2O_2$ + TTX on transfected HEK293 cells compared to cardiac myocytes. My results indicate that $H_2O_2$ cannot evoke the $I_{Na(P)}$ in cells expressing $Na_V1.5$ and, thus, the TTX-sensitive prolonged action potential recorded in other studies is likely the result of other VGSC isoforms in cardiac myocytes. The results also highlight the likely importance of β subunits in VGSC activation/inactivation, as dictated by the shifts in both my IV and voltage-dependence of inactivation curves between transfected HEK293 cells and myocytes. This study falls short in trying to elucidate $I_{Na(P)}$ in cardiac myocytes, and this is attributed to the low abundance of $Na_V1.1$ in myocytes as well as an insensitivity of $Na_V1.5$ to $H_2O_2$. Future studies, therefore, should directly compare the pharmacological and biophysical differences that might occur between transfected $Na_V1.1$-HEK293 with β1/ β2 subunits and transfected $Na_V1.5$-HEK293 with β1/ β3 subunits.

# References


Alzheimer C, Schwindt PC & Crill WE. (1993). Modal gating of Na+ channels as a mechanism of persistent Na+ current in pyramidal neurons from rat and cat sensorimotor cortex. *J Neurosci* **13,** 660-673.

Amitai Y. (1994). Membrane potential oscillations underlying firing patterns in neocortical neurons. *Neuroscience* **63,** 151-161.

Attwell D, Cohen I, Eisner D, Ohba M & Ojeda C. (1979). The steady state TTX-sensitive ("window") sodium current in cardiac Purkinje fibres. *Pflugers Arch* **379,** 137-142.

Barrington PL. (1994). Interactions of H2O2, EGTA and patch pipette recording methods in feline ventricular myocytes. *J Mol Cell Cardiol* **26,** 557-568.

Baruscotti M, Westenbroek R, Catterall WA, DiFrancesco D & Robinson RB. (1997). The newborn rabbit sino-atrial node expresses a neuronal type I-like Na+ channel. *J Physiol* **498,** 641-648.

Benndorf K, Boldt W & Nilius B. (1985). Sodium current in single myocardial mouse cells. *Pflugers Arch* **404,** 190-196.

Bennett PB, Yazawa K, Makita N & George AL, Jr. (1995). Molecular mechanism for an inherited cardiac arrhythmia. *Nature* **376,** 683-685.

Bentivoglio M, Bergamini E, Fabbri M, Andreoli C, Bartolini C, Cosmi D, Capasso V, Bottini P & Ambrosio G. (2008). [Obstructive sleep apnea syndrome and cardiovascular diseases]. *G Ital Cardiol (Rome)* **9,** 472-481.

Berman MF, Camardo JS, Robinson RB & Siegelbaum SA. (1989). Single sodium channels from canine ventricular myocytes: voltage dependence and relative rates of activation and inactivation. *J Physiol* **415,** 503-531.

Bezanilla F. (2000). The voltage sensor in voltage-dependent ion channels. *Physiol Rev* **80,** 555-592.

Bezanilla F & Armstrong CM. (1974). Gating currents of the sodium channels: three ways to block them. *Science* **183,** 753-754.

Bhatnagar A, Srivastava SK & Szabo G. (1990). Oxidative stress alters specific membrane currents in isolated cardiac myocytes. *Circ Res* **67,** 535-549.

Bodewei R, Hering S, Lemke B, Rosenshtraukh LV, Undrovinas AI & Wollenberger A. (1982). Characterization of the fast sodium current in isolated rat myocardial cells: simulation of the clamped membrane potential. *J Physiol* **325,** 301-315.

Brette F & Orchard CH. (2006). No apparent requirement for neuronal sodium channels in excitation-contraction coupling in rat ventricular myocytes. *Circ Res* **98,** 667-674.

Catterall WA. (1979). Binding of scorpion toxin to receptor sites associated with sodium channels in frog muscle. Correlation of voltage-dependent binding with activation. *J Gen Physiol* **74,** 375-391.

Catterall WA. (2000). From ionic currents to molecular mechanisms: the structure and function of voltage-gated sodium channels. *Neuron* **26,** 13-25.

Catterall WA, Goldin AL & Waxman SG. (2005). International Union of Pharmacology. XLVII. Nomenclature and structure-function relationships of voltage-gated sodium channels. *Pharmacol Rev* **57,** 397-409.

Cestele S, Qu Y, Rogers JC, Rochat H, Scheuer T & Catterall WA. (1998). Voltage sensor-trapping: enhanced activation of sodium channels by beta-scorpion toxin bound to the S3-S4 loop in domain II. *Neuron* **21,** 919-931.

Cestele S, Scheuer T, Mantegazza M, Rochat H & Catterall WA. (2001). Neutralization of gating charges in domain II of the sodium channel alpha subunit enhances voltage-sensor trapping by a beta-scorpion toxin. *J Gen Physiol* **118,** 291-302.

Costa MR & Catterall WA. (1984a). Cyclic AMP-dependent phosphorylation of the alpha subunit of the sodium channel in synaptic nerve ending particles. *J Biol Chem* **259,** 8210-8218.

Costa MR & Catterall WA. (1984b). Phosphorylation of the alpha subunit of the sodium channel by protein kinase C. *Cell Mol Neurobiol* **4,** 291-297.

Crill WE. (1996). Persistent sodium current in mammalian central neurons. *Annu Rev Physiol* **58,** 349-362.

Dhar Malhotra J, Chen C, Rivolta I, Abriel H, Malhotra R, Mattei LN, Brosius FC, Kass RS & Isom LL. (2001). Characterization of sodium channel alpha- and beta-subunits in rat and mouse cardiac myocytes. *Circulation* **103,** 1303-1310.

Docherty RJ & Farmer CE. (2009). The pharmacology of voltage-gated sodium channels in sensory neurones. *Handb Exp Pharmacol,* 519-561.

Dumaine R, Wang Q, Keating MT, Hartmann HA, Schwartz PJ, Brown AM & Kirsch GE. (1996). Multiple mechanisms of Na+ channel--linked long-QT syndrome. *Circ Res* **78,** 916-924.

Fahmi AI, Patel M, Stevens EB, Fowden AL, John JE, 3rd, Lee K, Pinnock R, Morgan K, Jackson AP & Vandenberg JI. (2001). The sodium channel beta-subunit SCN3b modulates the kinetics of SCN5a and is expressed heterogeneously in sheep heart. *J Physiol* **537,** 693-700.

Fearon IM & Brown ST. (2004). Acute and chronic hypoxia regulation of recombinant hNa(v)1.5 alpha subunits. *Biochem Biophys Res Commun* **324,** 1289-1295.

Ferrari R, Guardigli G, Mele D, Percoco GF, Ceconi C & Curello S. (2004). Oxidative stress during myocardial ischaemia and heart failure. *Curr Pharm Des* **10,** 1699-1711.

Fliss H. (1988). Oxidation of proteins in rat heart and lungs by polymorphonuclear leukocyte oxidants. *Mol Cell Biochem* **84,** 177-188.

Fozzard HA & Hanck DA. (1996). Structure and function of voltage-dependent sodium channels: comparison of brain II and cardiac isoforms. *Physiol Rev* **76,** 887-926.

Fozzard HA & Lipkind GM. (2010). The tetrodotoxin binding site is within the outer vestibule of the sodium channel. *Mar Drugs* **8,** 219-234.

Fraser H, Belardinelli L, Wang L, Light PE, McVeigh JJ & Clanachan AS. (2006). Ranolazine decreases diastolic calcium accumulation caused by ATX-II or ischemia in rat hearts. *J Mol Cell Cardiol* **41,** 1031-1038.

Frelin C, Cognard C, Vigne P & Lazdunski M. (1986). Tetrodotoxin-sensitive and tetrodotoxin-resistant $Na^+$ channels differ in their sensitivity to $Cd^{2+}$ and $Zn^{2+}$. *Eur J Pharmacol* **122,** 245-250.

French CR, Sah P, Buckett KJ & Gage PW. (1990). A voltage-dependent persistent sodium current in mammalian hippocampal neurons. *J Gen Physiol* **95,** 1139-1157.

Goldin AL. (1999). Diversity of mammalian voltage-gated sodium channels. *Ann N Y Acad Sci* **868,** 38-50.

Goldin AL. (2003). Mechanisms of sodium channel inactivation. *Curr Opin Neurobiol* **13,** 284-290.

Haigney MC, Lakatta EG, Stern MD & Silverman HS. (1994). Sodium channel blockade reduces hypoxic sodium loading and sodium-dependent calcium loading. *Circulation* **90,** 391-399.

Hartshorne RP, Messner DJ, Coppersmith JC & Catterall WA. (1982). The saxitoxin receptor of the sodium channel from rat brain. Evidence for two nonidentical beta subunits. *J Biol Chem* **257,** 13888-13891.

Haufe V, Cordeiro JM, Zimmer T, Wu YS, Schiccitano S, Benndorf K & Dumaine R. (2005). Contribution of neuronal sodium channels to the cardiac fast sodium current INa is greater in dog heart Purkinje fibers than in ventricles. *Cardiovasc Res* **65,** 117-127.

Heinemann SH, Terlau H & Imoto K. (1992a). Molecular basis for pharmacological differences between brain and cardiac sodium channels. *Pflugers Arch* **422,** 90-92.

Heinemann SH, Terlau H, Stuhmer W, Imoto K & Numa S. (1992b). Calcium channel characteristics conferred on the sodium channel by single mutations. *Nature* **356,** 441-443.

Hodgkin AL & Huxley AF. (1952). A quantitative description of membrane current and its application to conduction and excitation in nerve. *J Physiol* **117,** 500-544.

Hyslop PA, Hinshaw DB, Schraufstatter IU, Sklar LA, Spragg RG & Cochrane CG. (1986). Intracellular calcium homeostasis during hydrogen peroxide injury to cultured P388D1 cells. *J Cell Physiol* **129,** 356-366.

Isenberg G & Ravens U. (1984). The effects of the Anemonia sulcata toxin (ATX II) on membrane currents of isolated mammalian myocytes. *J Physiol* **357,** 127-149.

Jahnsen H & Llinas R. (1984). Electrophysiological properties of guinea-pig thalamic neurones: an in vitro study. *J Physiol* **349,** 205-226.

Josephson IR & Sperelakis N. (1989). Tetrodotoxin differentially blocks peak and steady-state sodium channel currents in early embryonic chick ventricular myocytes. *Pflugers Arch* **414,** 354-359.

Ju YK, Saint DA & Gage PW. (1996). Hypoxia increases persistent sodium current in rat ventricular myocytes. *J Physiol* **497 ( Pt 2),** 337-347.

Kalume F, Yu FH, Westenbroek RE, Scheuer T & Catterall WA. (2007). Reduced sodium current in Purkinje neurons from Nav1.1 mutant mice: implications for ataxia in severe myoclonic epilepsy in infancy. *J Neurosci* **27,** 11065-11074.

Kao CY & Walker SE. (1982). Active groups of saxitoxin and tetrodotoxin as deduced from actions of saxitoxin analogues on frog muscle and squid axon. *J Physiol* **323,** 619-637.

Ko SH, Lenkowski PW, Lee HC, Mounsey JP & Patel MK. (2005). Modulation of Na(v)1.5 by beta1-- and beta3-subunit co-expression in mammalian cells. *Pflugers Arch* **449,** 403-412.

Kunze DL, Lacerda AE, Wilson DL & Brown AM. (1985). Cardiac Na currents and the inactivating, reopening, and waiting properties of single cardiac Na channels. *J Gen Physiol* **86,** 691-719.

Lederer WJ & Tsien RW. (1976). Transient inward current underlying arrhythmogenic effects of cardiotonic steroids in Purkinje fibres. *J Physiol* **263,** 73-100.

Li M, West JW, Lai Y, Scheuer T & Catterall WA. (1992). Functional modulation of brain sodium channels by cAMP-dependent phosphorylation. *Neuron* **8,** 1151-1159.

Lipkind GM & Fozzard HA. (1994). A structural model of the tetrodotoxin and saxitoxin binding site of the Na+ channel. *Biophys J* **66,** 1-13.

Llinas R & Sugimori M. (1980). Electrophysiological properties of in vitro Purkinje cell somata in mammalian cerebellar slices. *J Physiol* **305,** 171-195.

Maier SK, Westenbroek RE, McCormick KA, Curtis R, Scheuer T & Catterall WA. (2004). Distinct subcellular localization of different sodium channel alpha and beta subunits in single ventricular myocytes from mouse heart. *Circulation* **109,** 1421-1427.

Maier SK, Westenbroek RE, Schenkman KA, Feigl EO, Scheuer T & Catterall WA. (2002). An unexpected role for brain-type sodium channels in coupling of cell surface depolarization to contraction in the heart. *Proc Natl Acad Sci U S A* **99,** 4073-4078.

Makielski JC, Sheets MF, Hanck DA, January CT & Fozzard HA. (1987). Sodium current in voltage clamped internally perfused canine cardiac Purkinje cells. *Biophys J* **52,** 1-11.

Makita N, Bennett PB & George AL, Jr. (1996). Molecular determinants of beta 1 subunit-induced gating modulation in voltage-dependent Na+ channels. *J Neurosci* **16,** 7117-7127.

Mekhfi H, Veksler V, Mateo P, Maupoil V, Rochette L & Ventura-Clapier R. (1996). Creatine kinase is the main target of reactive oxygen species in cardiac myofibrils. *Circ Res* **78,** 1016-1027.

Mozzi R, Andreoli V & Horrocks LA. (1993). Phosphatidylserine synthesis in rat cerebral cortex: effects of hypoxia, hypocapnia and development. *Mol Cell Biochem* **126,** 101-107.

Murayama K, Abbott NJ, Narahashi T & Shapiro BI. (1972). Effects of allethrin and Condylactis toxin on the kinetics of sodium conductance of crayfish axon membranes. *Comp Gen Pharmacol* **3,** 391-400.

Murphy BJ, Rossie S, De Jongh KS & Catterall WA. (1993). Identification of the sites of selective phosphorylation and dephosphorylation of the rat brain $Na^+$ channel alpha subunit by cAMP-dependent protein kinase and phosphoprotein phosphatases. *J Biol Chem* **268,** 27355-27362.

Murray KT, Anno T, Bennett PB & Hondeghem LM. (1990). Voltage clamp of the cardiac sodium current at 37 degrees C in physiologic solutions. *Biophys J* **57,** 607-613.

Narahashi T. (2008). Tetrodotoxin: a brief history. *Proc Jpn Acad Ser B Phys Biol Sci* **84,** 147-154.

Narahashi T, Moore JW & Poston RN. (1967). Tetrodotoxin derivatives: chemical structure and blockage of nerve membrane conductance. *Science* **156,** 976-979.

Narahashi T, Moore JW & Shapiro BI. (1969). Condylactis toxin: interaction with nerve membrane ionic conductances. *Science* **163,** 680-681.

Natarajan V, Taher MM, Roehm B, Parinandi NL, Schmid HH, Kiss Z & Garcia JG. (1993). Activation of endothelial cell phospholipase D by hydrogen peroxide and fatty acid hydroperoxide. *J Biol Chem* **268,** 930-937.

Noble D & Noble PJ. (2006). Late sodium current in the pathophysiology of cardiovascular disease: consequences of sodium-calcium overload. *Heart* **92 Suppl 4,** iv1-iv5.

Numann R, Catterall WA & Scheuer T. (1991). Functional modulation of brain sodium channels by protein kinase C phosphorylation. *Science* **254,** 115-118.

Palumbo EJ, Sweatt JD, Chen SJ & Klann E. (1992). Oxidation-induced persistent activation of protein kinase C in hippocampal homogenates. *Biochem Biophys Res Commun* **187,** 1439-1445.

Patlak JB & Ortiz M. (1985). Slow currents through single sodium channels of the adult rat heart. *J Gen Physiol* **86,** 89-104.

Pike MM, Kitakaze M & Marban E. (1990). 23Na-NMR measurements of intracellular sodium in intact perfused ferret hearts during ischemia and reperfusion. *Am J Physiol* **259,** H1767-1773.

Qu Y, Curtis R, Lawson D, Gilbride K, Ge P, DiStefano PS, Silos-Santiago I, Catterall WA & Scheuer T. (2001). Differential modulation of sodium channel gating and persistent sodium currents by the beta1, beta2, and beta3 subunits. *Mol Cell Neurosci* **18,** 570-580.

Ravens U. (1976). Electromechanical studies of an Anemonia sulcata toxin in mammalian cardiac muscle. *Naunyn Schmiedebergs Arch Pharmacol* **296,** 73-78.

Rogers JC, Qu Y, Tanada TN, Scheuer T & Catterall WA. (1996). Molecular determinants of high affinity binding of alpha-scorpion toxin and sea anemone toxin in the S3-S4 extracellular loop in domain IV of the $Na^+$ channel alpha subunit. *J Biol Chem* **271,** 15950-15962.

Rohl CA, Boeckman FA, Baker C, Scheuer T, Catterall WA & Klevit RE. (1999). Solution structure of the sodium channel inactivation gate. *Biochemistry* **38,** 855-861.

Rossie S & Catterall WA. (1987). Cyclic-AMP-dependent phosphorylation of voltage-sensitive sodium channels in primary cultures of rat brain neurons. *J Biol Chem* **262,** 12735-12744.

Rubin R & Farber JL. (1984). Mechanisms of the killing of cultured hepatocytes by hydrogen peroxide. *Arch Biochem Biophys* **228,** 450-459.

Saint DA. (2008). The cardiac persistent sodium current: an appealing therapeutic target? *Br J Pharmacol* **153,** 1133-1142.

Saint DA, Ju YK & Gage PW. (1992). A persistent sodium current in rat ventricular myocytes. *J Physiol* **453,** 219-231.

Sarkozy A & Brugada P. (2005). Sudden cardiac death: what is inside our genes? *Can J Cardiol* **21,** 1099-1110.

Schreibmayer W, Wallner M & Lotan I. (1994). Mechanism of modulation of single sodium channels from skeletal muscle by the beta 1-subunit from rat brain. *Pflugers Arch* **426,** 360-362.

Schwartz PJ, Priori SG, Spazzolini C, Moss AJ, Vincent GM, Napolitano C, Denjoy I, Guicheney P, Breithardt G, Keating MT, Towbin JA, Beggs AH, Brink P, Wilde AA, Toivonen L, Zareba W, Robinson JL, Timothy KW, Corfield V, Wattanasirichaigoon D, Corbett C, Haverkamp W, Schulze-Bahr E, Lehmann MH, Schwartz K, Coumel P & Bloise R. (2001). Genotype-phenotype correlation in the long-QT syndrome: gene-specific triggers for life-threatening arrhythmias. *Circulation* **103,** 89-95.

Shasby DM, Yorek M & Shasby SS. (1988). Exogenous oxidants initiate hydrolysis of endothelial cell inositol phospholipids. *Blood* **72,** 491-499.

Sipido KR, Callewaert G & Carmeliet E. (1995). Inhibition and rapid recovery of $Ca^{2+}$ current during $Ca^{2+}$ release from sarcoplasmic reticulum in guinea pig ventricular myocytes. *Circ Res* **76,** 102-109.

Song Y, Shryock JC & Belardinelli L. (2008). An increase of late sodium current induces delayed afterdepolarizations and sustained triggered activity in atrial myocytes. *Am J Physiol Heart Circ Physiol* **294,** H2031-2039.

Spragg RG, Hinshaw DB, Hyslop PA, Schraufstatter IU & Cochrane CG. (1985). Alterations in adenosine triphosphate and energy charge in cultured endothelial and P388D1 cells after oxidant injury. *J Clin Invest* **76,** 1471-1476.

Stuhmer W, Conti F, Suzuki H, Wang XD, Noda M, Yahagi N, Kubo H & Numa S. (1989). Structural parts involved in activation and inactivation of the sodium channel. *Nature* **339,** 597-603.

Wang Q, Shen J, Splawski I, Atkinson D, Li Z, Robinson JL, Moss AJ, Towbin JA & Keating MT. (1995). SCN5A mutations associated with an inherited cardiac arrhythmia, long QT syndrome. *Cell* **80,** 805-811.

Ward CA & Giles WR. (1997). Ionic mechanism of the effects of hydrogen peroxide in rat ventricular myocytes. *J Physiol* **500,** 631-642.

Ward CA & Moffat MP. (1995). Role of protein kinase C in mediating effects of hydrogen peroxide in guinea-pig ventricular myocytes. *J Mol Cell Cardiol* **27,** 1089-1097.

West JW, Numann R, Murphy BJ, Scheuer T & Catterall WA. (1991). A phosphorylation site in the Na+ channel required for modulation by protein kinase C. *Science* **254,** 866-868.

West JW, Patton DE, Scheuer T, Wang Y, Goldin AL & Catterall WA. (1992). A cluster of hydrophobic amino acid residues required for fast Na(+)-channel inactivation. *Proc Natl Acad Sci U S A* **89,** 10910-10914.

Yu FH & Catterall WA. (2003). Overview of the voltage-gated sodium channel family. *Genome Biol* **4,** 207.

Zweier JL, Flaherty JT & Weisfeldt ML. (1987). Direct measurement of free radical generation following reperfusion of ischemic myocardium. *Proc Natl Acad Sci U S A* **84,** 1404-1407.